CLM-R203

CLM-R203

UKAEA

Report

X-RAY CRYSTAL SPECTROSCOPY OF JET A DESIGN STUDY

M. G. HOBBY
N. J. PEACOCK
J. E. BATEMAN

CULHAM LABORATORY
Abingdon Oxfordshire

1980

C/18 Available from H. M. Stationery Office £4.00

CLM-R203

X-RAY CRYSTAL SPECTROSCOPY OF JET - A DESIGN STUDY

M G Hobby and N J Peacock
Culham Laboratory, Abingdon, Oxon, OX14 3DB, UK
(Euratom/UKAEA Fusion Association)

J E Bateman
Rutherford and Appleton Laboratories
Physics Apparatus Group
Instrumentation Division
Chilton, Didcot, Oxon.

February 1980
cms

ISBN 085311 087 5

CONTENTS

		Page No.
1.	AIM	1
2.	PURPOSE	1
3.	METHOD	2
4.	LIMITATIONS	3
5.	RANGE OF PLASMA PARAMETERS TO WHICH THE DIAGNOSTIC IS APPLICABLE	4
6.	SPECIFICATION OF THE INSTRUMENTATION	5
	6.1 General Concept	5
	6.2 Choice of Rowland Circle Size	7
	6.3 Criteria for Choice of Crystal, Diffraction Plane, and Viewing Angle	8
	6.4 Choice of Crystal Dictated by Wavelength and Viewing Angle	9
	6.5 Spatial Resolution, Crystal Aperture, and Passband	9
	6.6 Field of View and Spatial Scanning Range	11
	6.7 Length of Detector Regions	12
	6.8 Choice of Photoelectric Detector Dictated by Dispersion and Line Width	13
	6.9 Instrumental Resolving Power	14
	6.10 Sensitivity	16
7.	DETAILED SPECIFICATION OF THE PHOTOELECTRIC DETECTOR SYSTEM AND DATA HANDLING	18
	7.1 General Description	18
	7.2 The Electronic Functions	20
	7.3 Data Capture	21
	7.4 Overall Spectrometer Readout Configuration	22
	7.5 Data, Control, and Monitor Requirements for CODAS	22
	7.6 Overall Spectrometer Design	23
8.	SHIELDING REQUIREMENTS	24
	8.1 Magnetic and RF Shielding	24
	8.2 Operation in Hydrogen	24
	8.3 Operation in Deuterium - Tritium	26
	8.4 Operation in Deuterium	30
9.	PRELIMINARY APPRAISAL OF THE MECHANICAL DESIGN	31
10.	CALIBRATION AND ANCILLARY REQUIREMENTS	33
11.	PROBLEM AREAS AND DEVELOPMENT WORK	34
	TABLES 1 - 4	35
	FIGURES 1 - 11	
	LAYOUT DRAWINGS	
ANNEXE		
	BROAD-BAND CRYSTAL SPECTROSCOPY, A SURVEY INSTRUMENT FOR THE NON-ACTIVE PHASE OF JET	40
	FIGURES A1 - A4	

SYNOPSIS

Encouragement -

"The nature of the sun,
that passeth through pollutions"

BACON

Caveat -

....."the heaven's glorious sun
that will not be deep-searched by saucy looks"

SHAKESPEARE

This study describes the design and specification of a diagnostic system to measure x-ray line spectra from JET discharges with time-and space-resolution. Spectroscopy in the 1 - 15 Å region, which is the domain of crystal dispersion, can be expected to make a significant contribution to our understanding of the performance of JET since resonance lines involving K-shell electrons in all the metallic impurities expected (Ni, Cr, Fe, Mo and Ti) lie in this region, and will be the dominant emission line features in multikilovolt plasmas. Among others, the main parameters deduced will be ion temperatures from deconvolution of Doppler-broadened lines, and ion concentrations evaluated by Abel and tomographic inversion of radial profiles of emission intensity.

A Rowland circle, fully-focusing Johansson crystal mounting, used in reflection, will form the basis of the dispersion. Crystals are highly effective monochromators of x-rays rather than true broad-band spectrometers, so surveying a range of wavelengths conventionally involves scanning the crystal through a range of Bragg angles on a shot-to-shot basis. This is not suitable for JET where it would be preferred to collect all data on one pulse. It is proposed, instead, to record the full spectral range in a fixed-station spectrometer by means of a parallel battery of different crystals. A compact, small radius, high-aperture instrument viewing the plasma at fixed input and exit directions inside the biological shield results, and this allows the simultaneous observation of several pertinent transitions to a resolution of 1 part in 10^4 without the need for long scanning arms. Optional arrays of 4 such identical spectrometers in the horizontal viewing aspect, or 2 in the vertical aspect, are proposed, each element viewing a different chordal region. Angular scanning of only $\pm 5^{\circ}$ in a sequence of 3 discharges will provide spatial information from 90 - 100% of the plasma minor radius to a resolution of 10 cm. Photographic recording is envisaged initially (250 mm exposure), to be replaced in routine operation with multichannel, scanning photoelectric detectors for time-resolution ($\sim$ 10 ms).

The specification in terms of sensitivity, resolving power, and detector and data handling requirements is carefully detailed. Special attention is given to the considerable problems encountered in interfacing the spectrometer arrays to the torus vacuum system and in their disposition to the machine. Particular effort is devoted to evaluating shielding requirements during the active mode and a staged diagnostic is proposed to accommodate D-T operation. A single spectrometer option is presented for this mode.

1. AIM

This study describes the design and specification of a diagnostic system to measure the space-and time-resolved x-ray spectrum from JET discharges with high-resolution crystal spectrometers operating in the wavelength region 1-15Å.

2. PURPOSE

The object of the experiment is to obtain values of ion temperature T_i and ion concentration N_i as functions of plasma minor radius and time for a variety of high atomic number atoms of specific interest to JET. Measurements at x-ray wavelengths, for which the crystal spectroscopic technique is uniquely suited, are expected to make a significant contribution to our understanding of the performance of JET since resonance lines involving K-shell electrons in all the metal impurities likely to be present in JET lie in this region and will be the dominant line features at multikilovolt temperatures. Some or all of the following parameters will be deduced from the spectra

(i) Ion concentration profiles of high-Z impurities, profiles of Z_{eff} and their variation with time.

(ii) Ion diffusion rates.

(iii) Ion temperature T_i for high-Z impurity atoms such as Ni, Cr and Fe from the vacuum vessel walls, and Ti and possibily Mo from limiters.

(iv) Ion temperature T_i (thermalisation) for injected tracer atoms such as argon and neon.

(v) Changes in ion temperature during neutral injection, including the resolution of any two-component distributions, and asymmetries due to co- and counter-injection.

(vi) Changes in effective charge state and in radiation power loss due to charge transfer recombination during neutral injection.

(vii) Departures from steady-state (ionisation and recombination balance) predictions of ion populations.

It should be borne in mind that a useful and easily obtainable bonus may be gained in other areas such as measurements of electron temperature and density from line intensity ratios, and in the investigation of the thermodynamic state of the plasma as regards ionisation and recombination balance.

3. METHOD

Ion temperatures will be deduced from deconvolution of Doppler-broadened x-ray emission lines observed by time-resolved, spatial-scanning x-ray crystal spectroscopy. Ion concentration profiles will be deduced from Abel and tomographic inversion of radial profiles of emission intensity derived from chordal scans of the plasma. Rigorously, an inversion of the D-shaped plasma requires views in both horizontal and vertical directions simultaneously. Both the alternative modes of view offered as a solution to port allocation problems would then have to be implemented, either together or in succession in different periods.

Crystals are in fact highly effective monochromators of x-rays rather than true broad-band spectrometers, so surveying a range of wavelengths conventionally involves scanning the crystal through a range of Bragg angles on a shot-to-shot basis. This is not suitable for JET where it would be preferred to collect all data on one pulse. It is proposed, instead, to record the full spectral range in a fixed-station spectrometer by means of a parallel battery of different crystals in a compact, small radius, high-aperture instrument viewing the plasma at fixed input and exit directions.

Careful selection of the crystal spacings, mean viewing angle, and viewing spread around this angle will enable simultaneous observation of x-radiation in several pertinent transitions to a resolution of 1 part in 10^4 without the need for long scanning arms. Photographic recording is envisaged for initial time-integrated survey work and diagnosis of catastrophic disruptive pulses, to be replaced interchangeably, and eventually permanently for routine operation and in the active D-T phase, with multichannel, scanning photoelectric detectors for time-resolution ($\sim$ 10 ms). Angular scanning over $\pm 5^{\circ}$ in a sequence of three discharges will provide spatial information from 90-100% of the plasma minor radius depending on viewing aspect (to a resolution of 10 cm). An array of four spectrometers in the horizontal viewing aspect, or two in the vertical aspect, is proposed, each element in the array viewing a different radial region.

A conventional Rowland circle Johansson crystal mounting will be used. The crystal is here curved to twice the radius of the focusing circle and subsequently ground to the exact radius. The spectrum is viewed in reflection with a small radius circle. An unusual choice of viewing orientation with the Rowland circle axis lying orthogonal to the plasma toroidal axis exploits the inherent astigmatism of the optics to provide two simultaneous measurements

along the length of the emission line, each corresponding to a different space-resolved view of the plasma for one spectrometer setting.

4. LIMITATIONS

It is important to point out at this early stage that operational requirements peculiar to JET make it impossible to realise the full potential of the crystal spectroscopic technique even in the early, hydrogen phase of the machine's operation, and force an even further reduction in scope during the later, active phase. These restrictions will be discussed in detail later but it is worth summarising them here as an aid to understanding the structure of the study.

The very strict requirements on vacuum hygiene for equipment directly connected to the torus vacuum system, resulting particularly in the restriction on the maximum opening into the torus, are a severe limitation on a technique which depends on field of view for wavelength coverage. The vacuum cleanliness requirements can be met provided an entrance foil covers the aperture between spectrometer and torus, but a sufficient field of view can only be achieved through a first aperture $\sim$ 250 mm. The question of field of view is again paramount in the choice of entrance port. Alternative options for horizontal and large vertical ports are presented, though it should be understood that the latter must be a system of lower performance. The loss is in terms of reduced wavelength cover on one discharge and decreased spatial resolution, not in sensitivity or wavelength resolution. Of much more concern is the complete incompatibility of a system of several spectrometers requiring on the one hand close proximity to the machine for good spatial resolution, while on the other the massive shielding completely surrounding it for operation in the active phase of the machine's programme. There is no room to accommodate a concrete, lead-lined structure of up to 125 m^3 volume close to the torus. The solution proposed is that the diagnostic should also be phased; a full-specification system for operation in hydrogen, and also for the deuterium regime with minimal shielding, which is then adapted to the D-T active phase by reducing the number of elements to one unit and moving it back from the machine so that the concrete shell can be built round it. This can be accomplished simply by the provision of an extra flight-tube, a new port adaptor and a move to a horizontal port. There will be no alteration to the diagnostic instrument itself, though naturally it will be of lower specification again in terms of wavelength cover and space resolution. The choice of which radial view to retain from the original system should clearly be left until a full appraisal

of performance in the first phase has been obtained.

5. THE RANGE OF PLASMA PARAMETERS TO WHICH THE DIAGNOSTIC IS APPLICABLE

Electron temperatures T_e above 1 keV and densities n_e above 10^{13} cm^{-3} in discharges lasting for more than 10 ms ($n\tau \geq 10^{11}$) will result in a predominance of H-like, He-like and Li-like ion stages of the metallic atoms likely to be found in the JET plasma. These conditions are predicted as lower bounds for core regions ($r < a/2$) of the JET plasma in the standard performance 3.0 MA ohmic heating phase, and are bettered as mean plasma conditions for the 4.6 MA ohmic heating phase, neutral injection standard performance, and all other extended performance and extreme regimes listed in JET diagnostic memo No 1. Electron temperatures and densities above these minimum values will result in increased performance in terms of sensitivity. They will also alter the spectral distribution of the radiation to a large extent but not outwidth the instrumental specification. Radiation from these ions will become increasingly visible from the outer edges of the plasma as $\overline{T}_e$ and $\overline{n}_e$ increase.

The atoms of interest are Ni, Cr, Fe and Mo from the "Inconel" of the vacuum vessel, and Ti and Mo from the limiters. Resonance "optical" and "inner-shell" 1s-np transitions in all these atoms lie in the x-ray region between 0.5 and 3 Å (Table 1). Deliberate dopings of A or Ne would extend the range of atomic number probed down to 10, and the wavelength region to 14 Å. In outer, cooler regions of the plasma with temperatures below 1 keV, neon-like ion stages of the metallic atoms would predominate, and 2 - 3 transitions of these ions lie to slightly longer wavelengths (Table 1).

Doppler widths given by the relation

$$\frac{d\lambda}{\lambda} = 2.44 \times 10^{-3}\left(\frac{T_i}{M_i}\right)^{\frac{1}{2}} \quad \begin{cases} T_i \text{ in keV} \\ M_i \text{ in amu} \end{cases}$$

are shown in Table 2 for a range of ion temperatures above 1 keV for the elements of interest. Again a minimum of 1 keV is predicted for core regions of the standard 3.0 MA ohmic heated regime and for mean plasma conditions in all other regimes. It can be seen that resolving powers of greater than 4000 will be required to perform profile analysis on lines emitted by JET. This is well within the capability of good quality quartz crystals which have inherent resolving powers of $2 - 3 \times 10^4$. These are reduced by detector resolution and optical aberration of the mount, but typically only by factors of two or three.

Instrumental sensitivities with moderate f-numbers are such that 250 ms exposure photographic spectra can be obtained for atomic concentrations of 0.1% of the elements concerned. Indeed fluxes are sufficient to photoelectrically time-resolve spectra containing several lines with a resolution in the 50 ms range, and individual lines to 10 ms, indicating the ability to measure changes in T_i during neutral injection pulses.

During fault conditions of catastrophic runaway it will be impossible to provide enough shielding to prevent instantaneous gamma-ray background rates flooding photoelectric detectors. It will still be possible to use photographic recording in these conditions however.

6. SPECIFICATION OF THE INSTRUMENTATION REQUIRED

6.1 General Concept

The use of a Johansson curved and ground mounting in a conventional Rowland circle setting is proposed, Fig.1. This is a high-sensitivity, fully-focusing mount having no optical aberration due to the crystal aperture length W. There still remains a defocusing due to the aperture height h, but this can be kept to an acceptable level.

A reflection mode of operation is preferred. Observation in the transmission (Cauchois) mode would offer some advantage in that at the low Bragg angle required for optimum resolving power in this mode, the "straight-through" optical path would place the detectors further from the machine than the crystal, with a consequent amelioration of shielding and access problems. The presence of an absorbing barrier between input and exit beams would also reduce scattered long wavelength radiation. However these slight advantages are more than outweighed by the severe reduction in speed due to absorption in the crystal medium for radiation of wavelength greater than ~ 1 Å. This absorption also limits the range of crystals available, to those composed of low atomic number elements, and to those having good mechanical properties to enable the cutting and curving of extremely thin flexible lamellae. No such restrictions on atomic number exist for reflection optics; good mechanical properties, narrow diffraction widths for high resolving power, and suitable 2d-spacings being the only criteria to satisfy.

Resolving power and dispersion in reflection crystal optics are both better at large Bragg angles and in crystals with small 2d spacings. However, highly re-entrant optical paths are to be avoided since the detection system is

then situated closer to the torus. A compromise of moderate angles $\sim 50\text{-}60^{o}$ is recommended. Detectors must then be turned through a small angle from the tangent to view the incoming radiation normally, but this disadvantage is offset by the need to cover smaller dispersed distances l and the ability to shield the detector region adequately without obstructing the entrance beam.

Using microchannelplate multipliers with delay line readout, a flexible system of data-capture is proposed which permits spectra containing many lines to be sampled at 50-100 ms intervals, or individual line profiles at intervals of a few ms throughout the discharge.

Crystals are, in fact, highly effective monochromators of x-rays rather than true spectrometers, only diffracting rays of a given wavelength over a few seconds of arc close to the Bragg angle θ_B.

$$n\lambda = 2d \sin \theta_B \quad \text{where} \begin{cases} d \text{ is the spacing of the diffracting plane} \\ n \text{ is the diffraction order} \end{cases}$$

Observation of a range of wavelengths with a fixed crystal setting therefore requires that the source subtends a range of angles at the crystal surface. Surveying a large range of wavelengths with one crystal conventionally involves scanning the crystal, for a fixed input beam direction, through a range of Bragg angles $\Delta\theta$ and the detector through a range $2\Delta\theta$. Scanning in this manner on a shot-to-shot basis is not suitable for JET, however, where as much information as possible must be obtained on a single shot. A more tractable, though restrictive, solution is the one proposed here.

The wavelength ranges of interest will be covered by a parallel battery of crystals of different 2d-spacings (Table 3) all viewing a fixed mean input and exit direction i.e. each dispersion element is located on a common stack. Careful selection of the crystal spacings, mean viewing angle, and range of view about this angle enables the simultaneous observation of radiation from pertinent transitions in the most likely stages of high-Z impurity atoms which will exist in the plasma. No movement of optical beams is then required for wavelength scanning, though restrictions on field of view may require small adjustments ($\pm 3^{o}$) to accommodate the full range required. Ideally the battery should consist of as many crystals as are needed to cover the full wavelength range on one discharge. However this could be as many as eight, and would require an unacceptably large unobstructed aperture ($\sim$ 350 - 400 mm) into the torus. Even covering the spectrometer entrance with a thin foil of low permeability would still require the entrance to the torus from the fore-space

to be of this size, and it is now this aperture to which the vacuum specification applies. A battery of 3 crystals with associated detectors is thus proposed to view the plasma at any one time, but with the opportunity to select sequential groups of 3 crystals automatically from a permanent magazine of 6. (This still requires an aperture of 250 mm).

It is now necessary to consider the merits and drawbacks of the various options possible in the orientation of observation in order to provide a firm basis for a judgement of which is the most advantageous for JET. Provided the f-number W/R of the spectrometer and the field of view in the perpendicular dimension h are always filled by the source, sensitivity is completely independent of the distance from source to crystal L. However, the linear dimensions (orthogonal to the line of sight) of the volume filling the apertures will obviously increase with increasing L. Thus where constraints on access to the machine, and the adverse environment in which the apparatus may be placed define this distance, a maximum value of the f-number, and hence the sensitivity, will be set by the required spatial resolution. The resolving power is also dependent on the crystal height h so there may need to be compromise between sensitivity and wavelength resolution also.

The preferred viewing orientation is such that the Rowland circle axis of the spectrometer lies perpendicular to the plasma toroidal axis, Fig. 2(a). Two extremely important advantages accrue from this arrangement. Different wavelengths are now collected from regions lying along the plasma toroidal axis where gradients affecting emission characteristics are small. In addition the astigmatism of cylindrical grazing-incidence optics through the crystal height h can be exploited to give two spatially-resolved views across the minor radius of the plasma simultaneously, Fig.2(b),by discrete measurements along the length of the emission line. This immediately reduces the number of spatial scans to cover the whole plasma minor radius by a factor of two. (Note, this viewing orientation is not feasible on a vertical port because of access problems).

6.2 The Choice of Rowland Circle Size

The choice between large or small Rowland circle diameter values R for a given f-number W/R is determined in the main by convenience in the disposition of the spectrometer with respect to the machine. The benefits of a small compact spectrometer without a large vacuum chamber and long flaring input and exit arms to support are obvious, and the use of a small diameter R=75 cm is recommended. Optical paths within the spectrometer are then small, and inverse

dispersion (plate factor) is also lower so that bandpass distances and therefore detector lengths can be kept small. Sensitivity is not adversely affected since it depends on the ratio of W to R. A smaller diameter R for a fixed f-number is then a benefit since a small crystal is much easier to curve and grind to the high degree of precision required over the full length W than a large one. Defocusing aberrations, which are proportional to $(W/R)^2$ or $(h/R)^2$, also remain unchanged and crystal angular diffraction widths are only very slightly dependent on the degree of curvature. Thus resolving power does not decrease to any marked extent provided a high-spatial-resolution detector is specified to match the lower dispersion. The requirement ($\sim$ 0.035 mm) is within current technology of microchannelplate detectors.

6.3 Criteria for the Choice of Crystal, Diffraction Plane, and Viewing Angle

Crystals of high resolving power (small rocking curve width) are required for the main objective of measuring ion temperatures from the profiles of Doppler-broadened emission lines. Some alternative low-resolution (high-integrated-reflectivity) crystals may be specified for peak-intensity measurements when determining radial ionic concentration profiles.

The full wavelngth range, 0.5 - 15Å, should be covered by a parallel battery of a minimum number of crystals of different 2d spacings all viewing a single fixed mean input and exit direction. A high viewing angle is preferred for low optical aberrations, high resolution, and normal incidence on detectors, but access restrictions impose a compromise setting $\sim 50\text{-}60^{\circ}$. A small range of input angles about the mean is necessary for an adequate passband of wavelengths from each crystal and this is obtained by collecting radiation from a discrete volume of plasma of minimum cross-section. Groups of lines belonging to the same element should be recorded on one crystal. The individual lines from that element, and from elements seen by the other crystals, will be recorded at different input angles around the mean value. Thus the volumes from which the radiation from the various elements, and indeed different ion species of the same element, are collected will not in general be the same. This is not too great a problem in the preferred viewing orientation where these discrete volumes are distributed along the toroidal plasma axis. However this orientation cannot be obtained through the vertical port and there will be some blurring of wavelength information through the spatial resolution element of the plasma minor radius. By careful matching of the crystal to the line groups and mean viewing angle, the linear spread of viewed volumes can be kept to a minimum ($\sim$ 750 mm) in this mode. It should be pointed out that spatial

resolution of radial scans at a particular wavelength is in no way degraded by this spreading.

6.4 Choice of Crystal Dictated by Wavelengths and Viewing Angle

Consider the crystal reflections in Table 3 giving a mean observation angle of 53^{o} for the wavelengths denoted. Other mean angles could be chosen but this appears to be the only one giving a very high resolution reflection for Ni, a high-integrated-reflectivity alternative, and coverage of all the other wavelengths with good-resolution, good-reflectivity crystals. None of the neon-like lines of Fe, Cr or Ti are visible at convenient angles for this group of crystals so these are neglected in preference for those of Ni. There are eight first-choice, high-resolution reflections (seven crystals) backed up by six high-reflectivity alternatives. The total field of view required to cover the full range of wavelengths is 48.14^{o} - 57.61^{o}, i.e. approximately 10^{o}. The structure factor /F/ is a measure of the strength of the reflection.

6.5 Spatial Resolution, Crystal Aperture and Passband

A spatial element defined by apertures in the path from the plasma to the crystal merely delimits the full range of angles incident on the crystal and hence the full range of wavelengths sampled at one crystal setting.

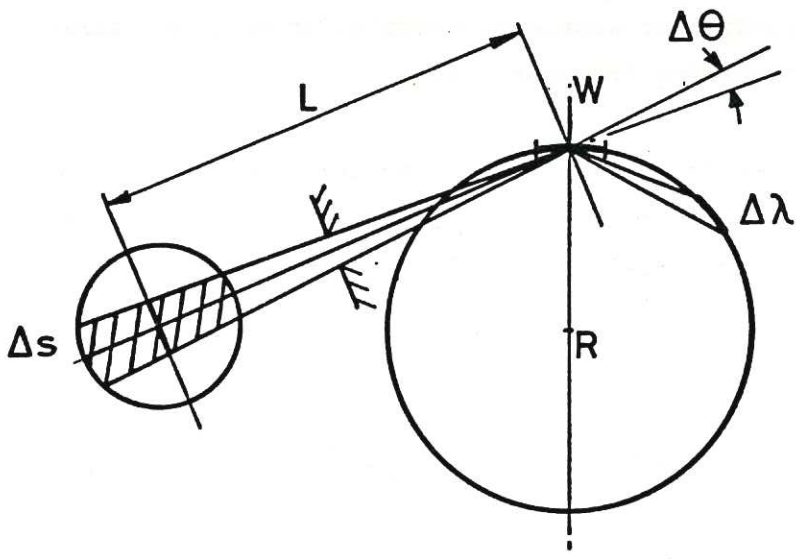

A more pertinent parameter for analytical work is the monochromatic space resolution element (MSRE), which is defined as the volume from which one particular wavelength is sampled uniformly by the whole crystal aperture W x h. This obviously depends on the f-number of the instrument W/R, the perpendicular divergence through h, and the distance to the source L.

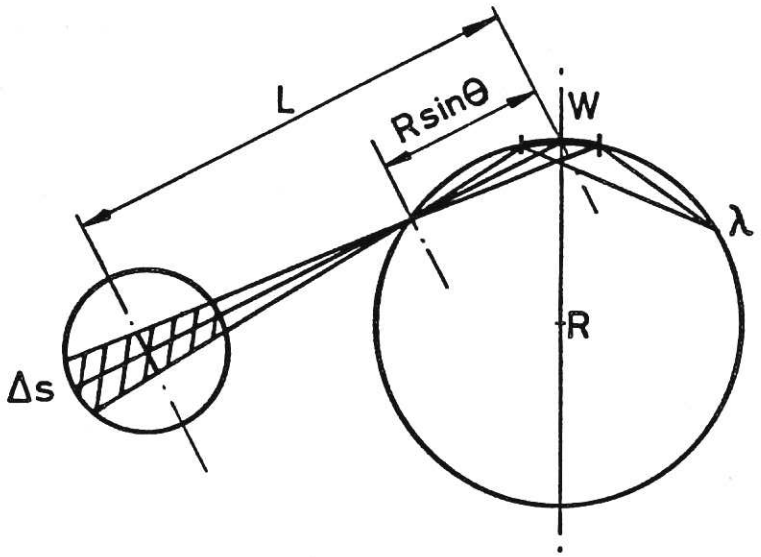

Where the space resolution element is defined as some canonical division of the plasma minor radius and the distance L is set by access constraints, the maximum crystal dimension W (or h depending on the viewing orientation), and hence the sensitivity, are then determined. There will obviously be cases where the full aperture dimensions must be reduced in order to provide either high spatial-or wavelength-resolution at the expense of sensitivity, and vice-versa where the spatial-or wavelength-resolution must be relaxed to gain more sensitivity by increasing the aperture.

For example, in the preferred viewing orientation, an 8.5 cm length of the plasma minor radius at a distance L=450 cm and a crystal to detector distance of 60 cm, specifies a crystal height

$$h = 8.5 \times 60/510 = 1.0 \text{ cm}$$

Conversely for the same crystal height at L = 725 cm in the active phase the space resolution element is 1.0 x 785/60 = 13 cm. There is no restriction on the spatial resolution along the toroidal axis, so the crystal length W can be set to any convenient value, say 3.0 cm. The field of view is then

$$\frac{W}{R} = \frac{30}{750} = 0.04 \text{ rad}$$
$$= 2.3^{o}$$
$$\equiv 15.6 \text{ cm at } L = 450 \text{ cm}$$

In the other viewing orientation for the vertical port application the space resolution element on the plasma minor radius becomes the MSRE as defined by the aperture length W. For example, with W = 3.0 cm as before, at L 500 cm in this case, the resolution element is 440 x 3.0/75 = 17.6 cm. The view through the crystal height h is now along the plasma toroidal axis and is unrestricted except for aperture width limitations.

A reasonable passband of wavelengths must always be maintained about the particular wavelength being observed. Thus the full volume which is sampled must of necessity be larger than the MSRE. A useful rule of thumb suggests that the dimension of the region from which radiation is sampled should not be much less than twice the MSRE length. The range of incident angles illuminating the crystal uniformly is then the same as that defined by the f-number. Thus the total angular field of view in the plane of dispersion should be no smaller than 4^{o} in this case. The total spread of incident angles will of course be greater than this but these other angles produce wings of decreasing illumination on the detector as less and less of the full aperture is used. Note also that the viewed volumes for individual lines are to a first approximation identical in size but not coincident in spatial location.

6.6 Field of View and Spatial Scanning Requirements

The full 10^{o} wavelength field together with the 3^{o} aperture field makes a total field of view requirement of 13^{o}. This will not be available through any port dimension. The full width of the horizontal port subtends only 8^{o} at the closest approachable machine radius R_M = 7.5 m (plasma axis to crystal distance of 4.5 m), and 4^{o} at R_M = 10 m during the active phase. A small wavelength scanning adjustment of the crystal battery and detector plane of the order of $\pm 5^{o}$ is thus required to accommodate this shortfall. In addition it should be remembered that only three crystals out of the battery of six will be in action on any one discharge because of the aperture restrictions. It is therefore an unavoidable fact of access and aperture problems that the potential wavelength cover of the instrument cannot be deployed on a single discharge. This point also applies to the vertical port application to an even greater extent since in the opposed orientation of this mode the wavelength field is also the spatial field. In a broad band wavelength-survey mode without spatial resolution a total field of 9^{o} is available at the "plasma axis to crystal" distance of 5.0 m, but with only two crystals because of the much narrower dimensions of this port. With spatial resolution, following the rule of thumb that the wavelength field should be no smaller than the aperture field, a total field of only 4^{o} obtains.

In the preferred viewing orientation through the horizontal port two simultaneous views of the vertical plasma minor radius at a resolution of the order of 10 cm are obtained through the crystal height for one setting. To cover the maximum plasma dimension, the long axis of the D-shaped plasma (210 cm), to this resolution on one discharge would therefore require simultaneous views on different chords by eleven spectrometers. This is clearly an unattainable goal. An array of four spectrometers is proposed, each viewing a different mean chordal region. A small spatial scanning adjustment within the spectrometer between successive discharges ($\pm 2.5^{o}$) would cover the whole of the vertical radius of the circular plasma (125 cm), and 200 cm of the vertical axis of the D-shaped plasma on a sequence of three discharges. The scheme is depicted in layouts C/4H(NA)/P, S. In the lower resolution vertical port application the whole of the minor radii of the D-shaped and circular plasmas (150 and 125 cm respectively) can be covered to a resolution of 18 cm with two spectrometers on a sequence of four discharges. The existing $\pm 4^{o}$ wavelength scan of the spectrometer would be used for this task in this orientation. The wavelength cover is severely limited in this mode but different regions of the spectrum can be covered on successive groups of four discharges. The spectrometers may also be required to look through different ports. The scheme is depicted in layouts C/2V(NA)P, S. The single spectrometer option for the active mode covers only 80 cm of the minor radius to a resolution of 13 cm on a sequence of three discharges. The scheme is depicted in layouts C/1H(A)/P,S.

6.7 Length of Detector Regions

The maximum spread of input angles to cover all the wavelengths of interest from the battery of crystals specified is from 48.14^{o} to 57.61^{o}. This is a range of 10^{o} with a mean value of 53^{o}. In a survey mode of operation, with no restriction on input angle range, a full angular spread of 10^{o} covers a detector region length of 131 mm for a Rowland circle diameter of 750 mm. To assist with machining this is rounded up to 135 mm centred on a mean viewing angle of 53^{o}. The overall cassette would consist of a stack of three parallel tracks of this length, each track covering the wavelength range from a different crystal in the selection from the battery. To view all the pertinent lines from a particular element in one crystal only a part of the overall length would need to be delimited. Fast x-ray film such as "Kodirex" in 35 mm wide roll form would be used. (Note - "Kodirex" is no longer manufactured but is replaced with "Kodak-NS" having similar characteristics).

ELEMENT	CRYSTAL	$\Delta\theta$	$\Delta\ell$ @ R = 750 mm
Ni	quartz $(22\bar{4}3)$	$49.34^{o} - 54.86^{o} = 5.52^{o}$	73 mm
Fe	quartz $(13\bar{4}0)$	49.33 - 55.29 = 5.95	78
Cr	quartz $(20\bar{2}3)$	49.79 - 56.38 = 6.59	87
Ti	quartz $(02\bar{2}2)$	48.40 - 55.35 = 6.95	91
A	quartz $(11\bar{2}0)$	53.47 - 54.81 = 1.34	18
Mo L-shell	quartz $(01\bar{1}1)$	48.15 - 53.96 = 5.81	76
Ne and Ni L-shell	beryl $(10\bar{1}0)$	49.51 - 57.44 = 7.93	104

Individual line groups in a particular ion species, or even close ion species, with a wavelength spread in the range 0.01 - 0.05 Å can be covered with photoelectric detectors which move freely over the whole detector region. The length of such a detector would depend on the maximum spread of the wavelengths in the group and the crystal used.

$$\lambda = 2d \sin\theta$$

$$d\lambda = 2d \cos\theta \, d\theta$$

$$dL = Rd\theta$$

$$= \frac{Rd\lambda}{2d\cos\theta}$$

For example, for the extreme case of the argon He-like group viewed in quartz $(11\bar{2}0)$ with R = 750 mm.

$$dL = \frac{750 \times 0.05}{4.913 \cos 54^{o}}$$

$$= 13 \text{ mm}$$

A standard microchannelplate face diameter is 25 mm.

6.8 Choice of Photoelectric Detector Dictated by Dispersion and Line Width

The plate factor (inverse dispersion) is given by

$$\Delta = \frac{2d \cos\theta}{nR} \quad \text{Å/mm} \qquad \text{where } \begin{cases} d \text{ is in Å} \\ R \text{ is in mm} \end{cases}$$

For a Rowland circle diameter of 750 mm the range of plate factors varies through

$$\Delta = \frac{2.030 \cos 53}{750} = 0.0016 \text{ Å/mm for Ni in quartz } (22\bar{4}3)$$

$$\Delta = \frac{4.913 \cos 53}{750} = 0.0039 \text{ Å/mm for A in quartz } (11\bar{2}0)$$

$$\Delta = \frac{15.955 \cos 53}{750} = 0.0128 \text{ Å/mm for Ne in beryl } (10\bar{1}0)$$

Doppler widths at the low T_i value of 1 keV likewise range through

$$d\lambda = 0.0005 \text{ Å for Ni}$$
$$d\lambda = 0.0015 \text{ Å for A}$$
$$d\lambda = 0.0066 \text{ Å for Ne}$$

The smallest linear widths that can be expected are thus of the order of 0.0005/0.0016 = 0.31 mm. Typical detector spatial definition therefore needs to be about an order of magnitude smaller than this to maintain resolution. Microchannelplates with channel diameters of 12.5 μm are commercially available now, though this high a resolution cannot be maintained through the readout system over the full 15 mm detector lengths specified in the previous section. A resolution of 30-40 μm is achievable, however, and is adequate for the present case.

6.9 Instrumental Resolving Power

$$\lambda = 2d \sin \theta$$
$$d\lambda = 2d \cos \theta \, d\theta$$

Instrumental resolving power $\left(\frac{\lambda}{d\lambda}\right)_I = \frac{\tan \theta}{d\theta}$

where $d\theta$ is a convolution of three parts

$d\theta_1$ the FWHM of the crystal diffraction pattern
$d\theta_2$ the FWHM of the geometrical aberration of the mount
$d\theta_3$ the FWHM of the detector resolution

At worst the three profiles will convolute dispersively so that the individual widths will add linearly.

(i) $d\theta_1$ depends on the crystal, the wavelength, and the surface preparation, varying from a few arc seconds to several arc minutes. For quartz a polished and etched surface finish followed by a non-mechanical polish will result in typical widths less than 10 arc seconds - 4.85×10^{-5} rad. (Table 4)

(ii) $d\theta_2$. In the Johansson mounting there is no geometrical aberration due to the crystal length W, but a height - dependent aberration given by

$$d\theta_2 = \frac{dL}{R} \text{ where } dL = \frac{h^2}{8R \sin\theta \cos\theta}$$

$$\text{i.e. } d\theta_2 = \frac{h^2}{8R^2 \sin\theta \cos\theta} \text{ rad}$$

$$= 4.62 \times 10^{-5} \text{ rad for } \begin{cases} h = 10 \text{ mm} \\ \theta = 53^o \end{cases}$$

(iii) $d\theta_3$ For the microchannelplate detector system dL = 0.035 mm.

$$\text{Thus } d\theta_3 = \frac{dL}{R} = \frac{0.035}{750} = 4.67 \times 10^{-5} \text{ rad}$$

The sensitivity of microchannelplates depends quite strongly on the angle of incidence of the radiation on the channels. At 2Å, for example, optimum quantum efficiency occurs at a glancing angle of 8^o to the channels. Plates are usually cut with the channels on a bias of this value to the plate face so that radiation incident normal to the face strikes the channels at the correct angle. For a disposition of the plate face tangential to the Rowland circle, radiation strikes the face at a mean angle of incidence of $90 - \bar{\theta}_B = 37^o$ (with a spread of $\pm 5^o$) in our case. A special bias of 30^o in the appropriate orientation would maintain optimum sensitivity for radiation incident at this angle (Fig. 3). Smaller standard biases would require the plate to be rotated a few degrees ε towards the incoming beam with a slight reduction in resolving power proportional to cos ε. Thus for a Lorentzian convolution $d\theta = 14.14 \times 10^{-5}$ rad and the resolving power is

$$(RP)_I = \frac{\tan 53}{14.14 \times 10^{-5}} = 9400$$

Similarly a Gaussian convolution would give a resolving power of

$$(RP)_I = \frac{\tan 53}{8.18 \times 10^{-5}} = 16,200$$

Higher resolving powers can be obtained at the expense of a slight drop in sensitivity by reducing the crystal height h (sensitivity falls as h while aberrations fall as h^2).

6.10 Sensitivity

The sensitivity relation for photographic recording is

$$\int D.dx = \frac{\tau.T(\lambda).P(\lambda).\ R\sin\theta.R_c}{(L + R\sin\theta).(L - R\sin\theta)} \cdot \int F(\lambda)d\lambda$$

$$= \frac{\tau.T(\lambda).P(\lambda).\ R\sin\theta.R_c}{(L + R\sin\theta)(L - R\sin\theta)} \cdot \frac{V}{4\pi} \int E(\lambda)d\lambda$$

$$= \frac{\tau.T(\lambda).P(\lambda).\ W.h.\ell.R_c}{4\pi R^2} \cdot \int E(\lambda)d\lambda$$

i.e. $$D_p = \frac{\tau.T(\lambda).P(\lambda).\ W.h.\ell.R_c}{4\pi R^2\ (dx)_{\frac{1}{2}}} \cdot \int E(\lambda)d$$

where $\int F(\lambda)d\lambda$ erg/str/s is the radiant intensity in a line at wavelength $\lambda\text{Å}$ from a volume V which fills the crystal aperture W x h (cm^2).

$\int E(\lambda)d\lambda$ erg/cm^3/s $= \frac{4\pi}{V} \int F(\lambda)d\lambda$ is the corresponding radiant power density.

$\int D.dx = Dp(dx)_{\frac{1}{2}}$ is the integrated photographic density in the line, where Dp is the peak density and $(dx)_{\frac{1}{2}}$ (cm) is the measured FWHM of the line.

τ s is the exposure time

$T(\lambda)$ is the transmission of the path at λ

$P(\lambda)$ density. $erg^{-1}.cm^2$ is the plate response factor of the emulsion at λ

R_c rad is the integrated reflectivity of the crystal at λ

L cm is the source to crystal distance

ℓ cm is the depth of the viewed volume

Consider the case of the Ni XXVII He-like $1s^2$ - $1s2p\ ^1P_1$ line at 1.59Å. The quartz $(22\bar{4}3)$ crystal has an aperture 3.0 x 1.0 cm^2 and a typical integrated reflectivity of 3 x 10^{-5} rad. X-ray film has a plate response factor of 1.6 for this wavelength and the exposure time is taken as 250 ms. An estimate of the radiant power density in this line can be obtained for JET conditions from calculations of Mertz, Cowan and Magee. Their results for the equivalent Fe XXV line for a 1% (0.01 n_e) doping of Fe in a plasma with n_e = 10^{14} cm^{-3} and T_e = 2.0 keV give a power loss of 2.3 x 10^5 erg/cm^3/s. Scaling to JET parameters of n_e = 3 x 10^{13} cm^{-3} and 0.1% doping for the same temperature gives a figure of 2.1 x 10^3 erg/cm^3/s. A simple coronal equilibrium calculation using the Van Regemorter formula for the same parameters yields an almost identical figure for the Ni XXVII line. The measured width of the line $(dx)_{\frac{1}{2}}$

will approximate the Doppler width of the line which at T_i = 2 keV is 0.00072/ 0.00169 = 0.043 cm. The depth of the emitting volume is taken as 125 cm corresponding to a hot core of radius a/2. The maximum photographic density expected is then

$$D_p = \frac{0.25 \times 1.0 \times 1.6 \times 3.0 \times 1.0 \times 125 \times 3 \times 10^{-5} \times 2.1 \times 10^{3}}{4\pi \times 75 \times 0.043}$$

$$= 0.24$$

This figure is just acceptable for single shot spectra. The alternative crystal with high integrated reflectivity ($\sim 1 \times 10^{-4}$) would give a three-fold improvement on this figure.

Photoelectrically the energy density in the line (of width $(dx)_{\frac{1}{2}}$ normal to the Rowland circle surface and therefore to the detector face) is

$$W = \frac{\tau.T(\lambda).W.h.\ell}{4\pi R\ (dx)_{\frac{1}{2}}} \cdot R_c \cdot \int E(\lambda)d\lambda \text{ erg/cm}^2$$

For photons of energy $h\nu$ erg, the photon density is then

$$U = \frac{\tau.T(\lambda).W.h.\ell}{4\pi R.h\nu.(dx)_{\frac{1}{2}}} \cdot R_c \cdot \int E(\lambda)d\lambda \text{ quanta/cm}^2$$

and the flux density

$$P = \frac{T(\lambda).W.h.\ell}{4\pi R.h\nu.(dx)_{\frac{1}{2}}} \cdot R_c \cdot \int E(\lambda)d\lambda \text{ quanta/cm}^2/\text{s}$$

For a detector of height ℓ', the flux in the line is thus

$$F = \frac{T(\lambda).W.h.\ell.\ell'}{4\pi R.h\nu} \cdot R_c \cdot \int E(\lambda)d\lambda \text{ quanta/s}$$

With the above conditions the flux density expected in the line ($h\nu$ = 1.24×10^{-8} erg) is

$$P = \frac{1.0 \times 3.0 \times 125 \times 1.0 \times 3.0 \times 10^{-5} \times 2.1 \times 10^{3}}{0.043 \times 1.24 \times 10^{-8} \times 4\pi \times 75}$$

$$= 4.7 \times 10^{7} \text{ quanta/cm}^2/\text{s}$$

With a detection efficiency of 2% this flux density represents a photoelectron emission (counting) rate in the detector of 9.4×10^5 electrons/cm^2/s. For a gain of 10^6 the charge collection rate is $9.4 \times 10^5 \cdot 10^6 \cdot 1.602 \times 10^{-19}$ coulombs/cm^2/s or 0.15 μamp/cm^2. This is within the current density limit for typical micochannelplates.

For a detector of height 1.0 cm the above flux density of 4.7×10^7 quanta/cm^2/s represents a flux of 2×10^6 quanta/s in the line, which at a detection efficiency of 2% represents a 4×10^4 Hz counting rate in the readout system.

7. DETAILED SPECIFICATION OF THE PHOTOELECTRIC DETECTOR SYSTEM AND DATA HANDLING REQUIREMENTS

7.1 General Description

With the crystal system described in the previous section intense x-ray spectra with flux densities approaching 10^8 quanta/cm^2/s in lines 1.0 cm high and 0.05 cm FWHM ($\sim 5 \times 10^6$ quanta/s/line), can be expected from JET discharges. Thus the opportunity exists to obtain time-resolved impurity spectra from JET on the time scale of a few ms provided a photoelectric detection system can be supplied with the following properties, (i) moderate quantum efficiency (~5%) (ii) spatial resolution of 35 µm FWHM (σ = 15µm), (iii) a counting rate capability of the order of 5×10^5 Hz.

Work done on an earlier system indicates that all these criteria can be met by means of a multichannel electron multiplier plate (MCP) detector with readout by means of the delay line technique. This system is based on the combination of two established techniques (a) the detection and location of soft x-rays by means of multichannel electron multiplier arrays (generally known as MCP's) and (b) the electronic readout of charge distributions (generally in multiwire proportional counters) by means of the delay line technique. In order for the latter device to function well a charge signal of $\sim 10^6$ electrons must be available to the delay line wand. This is achieved in the present device by menas of two cascaded MCP's which can produce electron gains (if need be) up to $\sim 10^8$, and so operate the delay line from the single electron pulses generated at the front face of an MCP by a soft x-ray. Fig. 4 shows a Cu $K\alpha_1\alpha_2$ spectrum at 1.5Å obtained with such a system. The delay line readout technique is chosen because of its simplicity (both in terms of the necessary hardware and the associated electronics), robustness, and ease of implementation. Particularly important is the ability of a delay line system to operate at high rates (up to $\sim 5 \times 10^5$ counts/second) without severe loss of spatial resolution. The delay line also provides a very linear readout characteristic.

In order to achieve the target spatial resolution of 35 µm (fwhm) or 15µm (standard deviation) over a useful length of 15 mm it is necessary to adapt the charge collection system from the more usual form in multiwire proportional

counter (MWPC) techniques. Delay lines generally can resolve 10^{-3} of their active length (in terms of the standard deviation σ) but the discriminator electronics and the delay line parameters indicate that this cannot be readily achieved on a 15 mm delay line. Consequently a spatial expansion by a factor of 10 is arranged by means of the printed circuit board design so that the readout takes place from a length of line 150 mm long. The observed resolution of $\sigma \sim 150$ µm on this line thus yields an effective 15 µm resolution on the channel plate surface.

Behind the special amplifier-discriminator units on the ends of the delay lines, the remaining electronics are conventional and commercially available.

Figure 5 gives a plan view of the x-ray readout system, viewed from the point of view of an incident x-ray. The principal elements of the system are indicated schematically.

(i) At the bottom of the board appears the channel plate assembly (two Mullard G25-25 devices) held in pyrophyllite mountings. The electrical connections from all four faces of the MCP are brought out on foil ribbons to the stand-off pillars surrounding the mounting.

(ii) The envelope of the electrical fan-out of the charge collection lines is shown. The printed circuit tracks expand by a factor of 10 from 4/mm under the channel plate to 4/cm under the delay line wand.

(iii) The series resistors (15 kΩ) placed in each signal line help to slow up the very fast charge pulse rise on the pads under the delay line. The MCP delivers the signal charge in $\sim$ 3 ns which causes ringing in the delay line. With the damping resistors in series the rise time at the delay line is $\sim$ 30 ns.

(iv) Each readout pad is returned to earth via a 220 kΩ resistor at the top edge of the readout board.

(v) The delay line wand is clamped in position across the readout pads. The wand is helically wound on a strip of glass-filled epoxy 25 mm wide and 1.6 mm thick The incremental delay is 2 ns/mm and the characteristic impedance is 820 Ω. The line is terminated at each end and coaxial cables take the signals away to the preamplifier-discriminator units via a vacuum leadthrough.

(vi) Three test points are provided so that test signals may be injected at each end and in the middle of the readout board. Figure 6 shows the test point arrangement in more detail. A fast negative going edge ($\lesssim$ 10 ns) of about 1 V will couple a suitable charge through the 10 pf capacitor onto a spread of 5 tracks centred on tracks 5, 45 and 85 (numbering from one end of the system). The spread of 5 tracks approximately simulates the spatial spread of the signal charge pulse.

(vii) Figure 6 shows a schematic sectional view of the channel plate assembly with the bias and test pulse networks also shown. The DC bias network is particularly simple, providing $\sim \frac{1}{3}$ of the applied volts across each channel plate with suitable collecting potential drops between the two plates and between the second plate and the readout array. In practice the system operates at around -2400 V overall with 800 V across each channel plate giving a charge gain of $\sim 10^6$. The collecting potential ($\sim$ 190 V across a gap of 1 mm) is chosen so that the final charge cloud spreads out over about 1 to 2 mm on the collecting array. The precise position of the x-ray impact is then recovered in the usual way be means of the centroid of the delay line pulse.

(viii) In order to operate at 10^6 charge gain the channel plates must be housed in a vacuum of 10^{-6} torr. An upper limit for operation is around 5×10^{-6} torr.

7.2 The Electronic Functions

Figure 7 shows the schematic arrangement of the electronics necessary for recording the x-ray events. The signal induced by the electron cloud on the delay line propagates both ways above the delay line from its point of origin to drive the amplifier-discriminator units at each end. A delay approximately equal to the total delay line length (500 ns) is inserted in the leg of the logic chain connected to the "STOP' input of the TAC. The 'START' signal goes direct. The analogue output pulse from the TAC is now proportional to $T_1 + T_D - T_2$. This shows that the system has a range of delays from 0 to 2 T_D and the incremental delay of the line has effectively been increased by a factor of 2. The TAC output pulse can be fed directly to a PHA so that a number versus position curve is immediately recorded for the incident x-ray distribution.

(i) The electrical specification of the delay line is - Z_0 = 820 Ω, incremental delay - 2 ns/mm and rise time $\sim$ 50 ns. It is important that the delay wand be placed symmetrically on the board so that the extreme ends are not used as pickup regions.

(ii) The basic requirement of the preamplifier-discriminator units is that the circuits yield a time resolution of better than 2 ns FWHM over a dynamic range of greater than 20 db in pulse height and over the whole length of the delay line. Generally the signals at the end of the delay line are $\sim$ 5 mV, a gain of $\sim$ 50 is employed in the preamplifier and the discriminator threshold set about 100 mV, Images of the amplified delay line pulses are available on the outputs marked A, $\overline{A}$ (50 Ω terminated).

7.3 Data Capture

An important requirement on the detector system is that statistically meaningful x-ray spectra must be acquired in short time intervals. Tests show that the limitation of the MCP current density lies at about 10^5 Hz per x-ray line and the global rate on the MCP (set by rate effects in the discriminators) at 10^6 Hz (i.e. 10 x-ray lines). Clearly a fairly sophisticated memory is required to permit data storage at this rate. Fortunately such a device is available in the form of the LeCroy Model 8810 histogramming memory. This device comes in a CAMAC module containing 16K of 16 bit words randomly addressable with a clock frequency of 1 MHz. Figure 8 shows how this system is implemented.

The time to amplitude converter (TAC) and pulse height analyser (PHA) of Figure 7 is replaced by a time to digital converter (TDC) which supplies the address to the histogramming memory whose location is incremented by a given event. The control module arranges for the appropriate dwell time on each spectrum and adds on the appropriate channel '0' address to the TDC output address. The control module is programmed via the CAMAC bus to execute predetermined scan periods which may be chosen at will. Given a data rate of $\sim 10^5$ Hz/line scan times as short as 1 ms will be possible.

Since the spatial resolution of the delay line system is $\sim$ 1 in 1000 of its length, it is suitable to choose 1024 as the maximum length of spectrum. The basic memory module is 16K words so only 16 spectra can be accumulated before the memory is full. The memory capacity per JET shot can be readily extended by redirecting the data stream to a second (and subsequent) 16K module. In many cases (for example in doppler broadening ion temperature measurements) it is unnecessary to store all 1024 channels of data. For fitting a doppler peak some 128 channels will be adequate and this implies that some 128 time samples can be performed before the 16K module is full. The relationship between time samples and storage is of course arbitrary and can be selected by means of the control module. The ultimate limit in respect of short time

samples is simply set by counting statistics. The control module will provide facilities for the necessary expansion or contraction of the stored spectrum.

The controlling computer will provide means of display and analysis of the spectra by means of suitable graphics facilities.

7.4 Overall Spectrometer Readout Configuration

It is proposed to have a battery of crystals in each spectrometer (up to 6), three of which produce a spectrum in a different wavelength range on any one shot. In addition each crystal will produce two spatially-resolved views of the plasma. The current proposal is thus to have 3 double readout systems. Each double system uses a single 20 mm diameter channel plate assembly permitting two vertically separated readout areas each $\sim$ 10 mm x 15 mm. The double system is mounted with its two fanout boards and delay lines so as to scan around the Rowland circle independently of the other double units. The overall depth of each pair of detectors would be $\sim$ 40 mm permitting stacking of the readouts within a reasonable vacuum chamber.

The electronic dispositions would consist of preamplifiers with the vacuum system and discriminator modules placed on the vacuum system wall. The TDC, control module and fast memory will be housed in a CAMAC crate requiring 5-6 CAMAC slots.

7.5 Data, Monitor and Control Requirements for CODAS

The total data, control and monitor requirements for one spectroscopic unit (one spectrometer) will consist of

1 shutter control 2 gate valve controls (diagnostic isolation) 7 movement (adjustment) controls	10 control levels
1 shutter monitor 2 gate valve monitors 7 movement monitors	10 monitor levels
6 data levels	6 data levels

The shutter and gate valve controls will be linked to the main timing sequences of the machine, the latter being enabled only by satisfactory vacuum status. Each data level is a pulse-counting system, storing in part (1024 words) of a randomly-addressable histogramming memory, digitised events arriving at a rate of up to 5×10^6 Hz during a time block of variable duration from 1 ms upwards. A sequence of 16 such time blocks, not necessarily consecutive, would

be counted into successive parts of the 16k word memory throughout the JET pulse. The duration and spacing of the time blocks will be controlled independently.

Word storage required:

16	x	1024	x	6	=	6 x 16k words/shot
Time Block		Memory Division (spectrum)		Levels		(10^5 words/shot)

Each word would not contain more than 10^4 counts, so 16 bit words would suffice.

Bit storage required: = 16 x 6 x 16k bits/shot
= 1.5×10^6 bits/shot

If spectroscopic units are to be multiplexed to give greater spatial cover during one shot up to four spectroscopic units may be required.

TOTAL WORD STORAGE	=	24 x 16k words/shot
	=	4×10^5 words/shot
TOTAL BIT STORAGE	=	6×10^6 bits/shot

Software will require to be developed for control and Abel and Tomographic inversion routines, and for deconvolution of Doppler-and instrumental-broadened profiles.

7.6 Overall Spectrometer Design

The overall configuration of the mechanical and optical components of the spectrometer is depicted in layout C/SOC. This is a representation only, to illustrate the disposition of the parts and does not constitute a firm design.

8. SHIELDING REQUIREMENTS

The problems of shielding instrumentation not only from neutrons and gamma-rays but from magnetic fields and radio frequency interference need to be considered. In the light of the recommendation to phase the diagnostic to deal initially with operation in hydrogen and then with the active operation in deuterium and deuterium-tritium it is convenient to discuss the neutron and gamma-ray shielding for the various phases separately. Magnetic field and RF interference problems are common to all operating regimes and are discussed in isolation first.

8.1 Magnetic and RF Interference Shielding

The detector regions will be at machine radii of 7.4 and 10 m respectively in the two cases of horizontal port disposition, and at a vertical distance below the equatorial axis of 5.0 m in the vertical port applicaiton. In none of these positions will the stray toroidal magnetic field be other than negligible. For the horizontal port settings poloidal field strengths in the median plane are of the order of 300 gauss and 80 gauss respectively at these distances for I_p = 4.8 MA. No maps of field strength in the vertical direction between the limbs are available though estimates from flux maps in the plane of the limb suggest upper limits between 1.4 kgauss 4.0 m below the equatorial axis, and 150 gauss 6.5 m below, at machine radius R_M = 3.0 m. A value of 300 gauss is taken as a working figure for this port setting.

Microchannelplates are not very sensitive to magnetic fields and provided a value of 100 to 200 gauss is not exceeded shielding is probably unnecessary. In the event of a larger ambient field, multiple mumetal screens will safely reduce the field to an acceptable level.

Radio frequency interference, on the other hand, is likely to be a problem. Small (mvolt), fast (20 MHz) electronic signals are being processed and considerable pains will be required to isolate the system in the JET environment to prevent undesirable RF corruption.

No problems will be encountered during photographic recording obviously.

8.2 Operation in Hydrogen

Detection of x-rays in a microchannelplate takes place in a very thin surface layer, and hence the sensitivity of the device to all types of neutral particles (x-rays, neutrons, gamma-rays etc) is in the ratio of the appropriate

cross-sections. In the MeV range the gamma-ray cross-section in the active layer is of the order of 10 barns while for x-rays of a few keV the cross-section is of the order of 10^5 barns. Thus the detector is $\sim 10^{-4}$ as sensitive for MeV gamma-rays as for keV x-rays. With fluxes of 10^8 x-rays/cm^2/s incident on the detector, if the background noise is not to exceed 1% of this figure, the gamma-ray flux must not exceed 10^{10} quanta/cm^2/s. However such a global rate induced in the detector (the x-rays are in discrete lines while the gamma-rays are isotropic) would represent a serious current loading. Background fluxes at least a further two orders of magnitude lower at 10^8 quanta/cm^2/s are required for an acceptable level.

For photographic recording the situation is less critical, since, though the relative sensitivities are not so favourable, an integrated uniform background is less troublesome. Fluences of gamma-rays below 10^8 quanta/cm^2 would be an acceptable level also.

In normal low density operation in hydrogen the hard x-ray (gamma-ray) exposure rate due to runaway electron bremsstrahlung is calculated as 20 R/yr, or 2×10^{-3} R/pulse, 13 m from the torus axis. This scales to 7×10^{-4} R/s during a 10 s pulse, 7 m from the torus axis. A worst case from a shielding point of view (half-thickness of lead is a maximum at 3 MeV, Fig. 9) assumes that this exposure rate is all due to 3 MeV gamma-rays, the inductive energy being converted to 3 MeV electrons. The conversion to fluxes, Fig. 10, then gives

$$\begin{aligned} F_{3MeV} &= 7 \times 10^{-4} \text{ R/s} \\ &= 7 \times 10^{-4} \times 3.6 \times 10^{6} \text{ mR/hr} \\ &= 7 \times 10^{-4} \times 3.6 \times 10^{6} \times 2.5 \times 10^{2} \text{ quanta/cm}^2\text{/s} \\ &= 6.3 \times 10^{5} \text{ quanta/cm}^2\text{/s} \end{aligned}$$

This is well below the fluxes specified as acceptable for photoelectric recording and in a 10 s pulse well below the integrated density acceptable for photographic recording. Shielding is probably unnecessary for normal operation therefore.

However, under fault conditions the gamma-ray exposure rate is calculated at 500 R/yr, or 10 R/pulse, 13 m from the torus axis. The pulse length for an abrupt disruption of this sort would be very short ($\sim$ 1 ms) so the instantaneous exposure rate during a fault could be incredibly high at 10^4 R/s. This is difficult to shield against from a background point of view photoelectrically

and such pulses may be undiagnosable by this means. The integrated dose of 500 R/yr is equivalent to 3×10^{10} quanta/cm^2/pulse 7 m from the machine axis (50 such pulses a year). Some 15 cm of lead (ten half-lengths) would reduce this density by 10^3 to an acceptable level of 3×10^7 quanta/cm^2/pulse for photographic recording. Provision should therefore be made even in this phase of operation to provide shielding of this depth. The beams of gamma-rays would be directional to a certain extent and this thickness would only be required between the detector and the machine.

There will be some yield of photoneutrons even in this phase due to runaway electrons accelerated up to 15 MeV. The dose rates will be too small to produce background problems though it will still be necessary to take account of integrated fluxes for damage to instrumentation in the long term. The calculated photoneutron dose is 0.8 R/yr for normal and disruptive pulses together. This is due to an equivalent flux of 1 MeV neutrons 7 m from the machine axis of

$$F = \frac{0.8}{4 \times 10^{-9}} \times \left(\frac{13}{7}\right)^2$$

$$= 6.9 \times 10^8 \text{ neutrons/cm}^2\text{/yr}$$

This integrates to 4×10^9 neutrons/cm^2 over the six year lifetime of the machine.

8.3 Operation in Deuterium-Tritium

In addition to the gamma-ray background ($\sim 6 \times 10^5$ quanta/cm^2/s) produced in normal operation by runaway electrons as discussed in the previous section (ignoring the catastrophic disruptive phase as undiagnosable), an intense isotropic flux of fast neutrons will be present throughout the torus hall. Three additional problems become apparent -

(1) a background induced in the detector by the neutron flux itself and the accompanying gamma-ray flux,

(2) activation of the materials of the detection system, and

(3) radiation damage to these materials.

(1) Radiation-Induced Background

Fast neutrons can produce an enormous range of interactions in materials from elastic and inelastic scattering to (n, γ),(n, p) and other reactions. However the bulk of the total cross-section in this region is in the elastic

process which also causes most trouble in that the recoils are densely ionising and can leave all their energy in the detector. This is not too great a problem in a pulse-counting system such as this where only the event is being detected not the integrated deposited energy. It is nevertheless a worst case to assume that all the neutron interactions with the active layer of the micro-channelplate are via elastic scattering. Elastic scattering cross-sections for most high-Z materials (Pb) lie in the range of a few barns. Thus the detector is of the order of 10^{-5} times as sensitive for fast neutrons as for keV x-rays. As before, if background noise is not to exceed 1% of the 10^{8} quanta/cm^2/s flux of x-rays, and global rates are not to present a serious current limitation, the neutron flux must not exceed 10^{9} neutrons/cm^2/s .

In D-T operation the maximum neutron yield is specified as 10^{24} over a two year period, or 5×10^{23} per year in 5000 pulses. Each pulse will last for 10 s , giving a production rate of 10^{19} neutrons/s.

Neutron fluxes in a range of energy groups have been modelled for various sectors of the torus hall from the calculated D-T neutron yield. Since the main application here is instrument damage the fluxes have been reduced to equivalent 1 MeV fluxes which give the same displacement rate in silicon. However, it is important to remember that for shielding purposes the bulk of this flux, particularly in unobstructed sectors such as (13 , n) and below the machine, will be be in the 10 to 14 MeV range. Dose rate has then been derived for one specific sector (12, 13) by converting from neutrons/cm^2 to Rad with the factor 4×10^{-9}. The orginally modelled fluxes in D-T operation have been increased by a factor of two to account for less efficient shielding in a modified support structure.

The maximum specified dose rate in D-T of 1.2×10^{7} Rad/yr in sector (12, 13) is equivalent to a 1 MeV flux of 3×10^{15} neutrons/cm^2/yr, or 6×10^{10} neutrons/cm^2/s (5000 x 10 s pulses). A more relevant flux in this case would be that for an unobstructed position say (13, 13) or at worst (13, 12). The equivalent flux in sector (13, 12) is 1.23×10^{16} n/cm^2/yr (4.9×10^{7} Rad/yr), or 2.46×10^{11} n/cm^2/s. To reduce this flux below the acceptable level of 10^{9} n/cm^2/s a factor of 10^{3} in shielding must be obtained. Fig. 11 shows this requires $\sim$ 100 cm of concrete for 14 - 15 MeV neutrons.

In D-T operation gamma-rays result from the interaction of the neutron flux with the vacuum vessel, coils, shielding and support structure via inelastic scattering and capture reactions, with the former dominating for

borated structures. An estimated maximum exposure rate of 10^7 R/yr is calculated for sector (12, 13) of the torus model. This includes the position proposed for the spectrometer in this phase. Again assuming a worst case for shielding purposes this exposure rate is equivalent to a 3 MeV gamma-ray flux of

$$F_{3\ MeV} = 10^7 \times 3.6 \times 10^6 \times 2.5 \times 10^2$$

$$= 9.0 \times 10^{15}\ \text{quanta/cm}^2\text{/yr}$$

$$= 1.8 \times 10^{11}\ \text{quanta/cm}^2\text{/s}$$

To reduce this to the acceptable level of 10^8 quanta/cm^2/s a factor of 10^3 in shielding must be obtained. Again 15 cm, or ten half-thicknesses, of lead would produce the requisite effect.

The gamma-rays from runaway electrons in normal operation are negligible in this context. However it is important to prevent thermal neutrons reaching the detector both from the noise aspect (thermal cross-sections are large at $\sim 10^4$ barns) and the activation aspect. Therefore it is as well to introduce a thermal neutron absorber (typically boron) into the concrete shielding and put a thin ($\sim$ 1 mm) cadmium screen as an inner skin. These processes generate gamma-rays of 0.4 to 1.5 MeV but the 15 cm of lead already required, used as an inner shield, would offer adequate protection here also (fifteen half-lengths for this energy range). It is also well known that composite shielding is much more efficient than single-component types.

(2) Activation

All parts of the system are liable to become activated but clearly activation of the microchannelplate is the most sensitive problem as this can lead to long-term noise. Only the thermal part of the neutron spectrum can contribute to the activation through the capture cross-section. The proportion of the spectrum which is thermal is almost totally dependent on the JET environment, the more shielding there is the more thermal neutrons there will be.

Consider a pulse of N_o thermal neutrons/cm^2 hitting the detector. The number of excited nuclei produced will be

$$\frac{N_o . N_A . \sigma . \rho . x}{A} \ / \ \text{cm}^2$$

where N_A is Avagadro's No

A is the gm atomic wt

x is the thickness (cm)

ρ is the density (gm/cm^3)

σ is the cross-section (cm)

The counting rate resulting from this population is

$$\frac{N_o . N_A . \sigma . \rho . x \log_e 2}{A . T_{\frac{1}{2}}}$$

where $T_{\frac{1}{2}}$ is the half-life of the state concerned

For the microchannelplate system where PbO is the major constituent of the active layer

$$\text{Activity} \sim \frac{N_o . \sigma . 10^{-5}}{T_{\frac{1}{2}}} \quad \text{counts/cm}^2\text{/s} \qquad \begin{cases} \sigma \text{ in barns} \\ T_{\frac{1}{2}} \text{ in s} \end{cases}$$

The $^{208}Pb(n,\gamma)^{209}$ reaction is the relevant one here so $\sigma \sim 10$ barns and $T_{\frac{1}{2}}$ is 1.2×10^4 s (3.3h).

$$\text{Activity} = N_o . 8 \times 10^{-9} \text{ counts/cm}^2\text{/sec}$$

To keep the noise level below the 1% level of the 10^8 quanta/cm^2/s x-ray flux and the global levels below current limits the activity should not exceed 10^4 counts/cm^2/s. That is the flux of slow neutrons should not exceed 1.2×10^{12} neutrons/cm^2/s. Such a flux of slow neutrons is many orders of magnitude above what one could anticipate in the worst case. At worst one would expect a factor of 10^{-4} of the 2.5×10^{12} neutrons/cm^2/pulse to thermalise.

Slow decay isotopes with half-lives of a few years would only slowly build up activity to the unacceptable level during many thousands of shots of this intensity and should not become a problem. Nevertheless it would be better to try to avoid materials of this nature in the spectrometer system. Steels are particularly bad in this respect and should be avoided in preference for light aluminium alloys.

A concomitant problem is absorption of tritium in the active layers of the detectors. Tritium being a β-emitter, this could also lead to build up of background noise in detectors, but this is not treated here as the spectrometer

parts will be isolated from the torus vacuum system by a low permeability foil.

(3) Radiation Damage

The materials of the detection system including components of the head amplifiers will start to show effects of radiation damage after fluences in the range 10^{13} - 10^{14} neutrons/cm^2. The integrated fluence over the lifetime of the machine, summing the contributions from the photoneutrons in all phases, 4 x 10^9/cm^2; from the two years of shielded deuterium operation, at most 10^{12}/cm^2 depending on the site chosen; and from two yeárs of deuterium - tritium operation, 2.5 x 10^{13}/cm^2 is thus within this range but dominated by the D-T operation. It would appear then that destruction of the device by radiation will be commensurate with the lifetime of the machine and is thus not likely to be a problem.

8.4 Operation in Deuterium

In D-D operation the maximum neutron yield is set at 10^{20} per year in order to limit activation before proceeding to D-T. This will be obtained in 3000 low-level pulses of 2.5 s, each giving 1.3 x 10^{16} neutrons/s, or 200 high-level pulses of 10 s at 5 x 10^{16} neutrons/s. The original scaling factors from D-T fluxes to account for the lower yield and lower energy giving fewer gamma-rays from inelastic scatter (5 x 10^{-4} for neutrons and 10^{-4} for gamma-rays) are further altered to 10^{-4} for neutrons and 2 x 10^{-5} for x-gamma-rays to account for the reduction in total yield from 10^{21} to 2 x 10^{20}. The shielding specified for D-T operation is therefore more than adequate protection here for fluxes reduced by these amounts if the decision is to move the spectrometer back for this phase also. From a radiation damage point of view the maximum neutron dose rate is specified as 1200 Rad/yr, or 3 x 10^{11} neutrons/cm^2/yr in sector (12, 13). The corresponding flux in sector (13, 12) would be 1.23 x 10^{12} neutrons/cm^2/yr giving a total fluence over the two years operation of 2.5 x 10^{12} neutrons/cm^2. With the shielding factor of 10^3 the actual fluence would be 2.5 x 10^9 neutrons/cm^2.

It is appropriate at this point to enquire whether operation in D-D might be feasible without moving to the larger distance position, by providing the minimum shielding that space will allow. The estimated gamma-ray exposure rate is 200 R/yr in sector (12, 13). For a position closer to the machine corresponding to the vertical port setting this is equivalent to a 3 MeV gamma-ray flux of 6.2 x 10^{11} quanta/cm^2/yr, or 10^8 quanta/cm^2/s, for low-level pulses and 3.1 x 10^8 quanta/cm^2/s for high-level pulses. The 15 cm of lead already proposed for the hydrogen phase would be adequate here also.

Considering the vertical port setting as a worst case, since machine shielding is a minimum here, and using the neutron fluxes pertaining to the unobstructed sector (13, 10) as more relevant to this setting, the 1 MeV equivalent flux of neutrons here would be 5.72×10^{12} n/cm^2/yr, or 9.5×10^{8} n/cm^2/s, during low-level pulses and 2.9×10^{9} n/cm^2/s, during high-level pulses. To reduce these fluxes by an order of magnitude would be sufficient and this can be achieved for 3 MeV neutrons with a cladding of 15 to 20 cm of borated polyethylene. Again the full shield should consist of a composite of borated polyethylene, cadmium and lead.

The total accumulated fluence in the two year period would be of the order of 10^{12} neutrons/cm^2.

9. PRELIMINARY APPRAISAL OF THE MECHANICAL DESIGN

It will have become apparent from the preceding sections that a large field of view is a "sine qua non" for crystal spectroscopy. An adequate field for the 'full' specification system can only be obtained through a (shared) horizontal port: the large vertical port barely provides enough field, even at its widest opening of 200 mm, for the monochromatic aperture of the crystal alone. A system of much reduced specification using two crystals to view two small selected wavelength regions on one discharge can be designed to use the vertical ports, but then only in the non-preferred orientation at reduced spatial resolution. The chosen wavelength regions can be altered on successive pulses but it is suggested that the prime candidates should be the Ni and Ti He-like groups. Both spectrometers may be fitted to a single vertical port but access will be very cramped as the lines of sight to cover the full plasma minor radius must all pass through the widest part of the available opening. It may therefore be necessary to mount each spectrometer on a separate port. Some of the neighbouring small vertical ports may need to be sacrificed as well. Spatial scanning over four discharges will be required to build up a full radial profile.

A large, massively shielded array in the active phase in incompatible with close access to the machine. A single spectrometer system of reduced specification in terms of spatial resolution and wavelength cover is therefore proposed for this phase. It is sited further back from the machine, again sharing a horizontal port, and a concrete and lead shield built round it.

In the following layouts the spectrometer optical component configuration is depicted under the heading

Spectrometer optical configuration, C/SOC

and the mechanical structures for the three cases of observation, in plan and section, under the titles

Four spectroscopic units, horizontal port application, non active phase
C/4H(NA)/P, S

Two spectroscopic units, vertical port application, non active phase
C/2V(NA)/P, S

One spectroscopic unit, horizontal port application, active phase
C/1H(A)/P, S

The first two are alternatives for the initial phases of operation while the third is the only one possible for the active phase.

The interfaces with the machine, the vacuum pumping requirements with gate-valve sizes and dispositions, and the size and location of the diagnostic are clearly indicated in the layouts and will not be elaborated on.

No part of a spectrometer body will be able to withstand vacuum baking to 300^{o}C, though this is acceptable for the containing vacuum tank, flight tubes and diagnostic valve. Since the spectrometer parts will always be separated from the Torus vacuum by an isolating foil window this is not thought to violate the vacuum specifications. All pumping systems will be tritium compatible with JET specifications yet to be issued, and extreme care will require to be taken in the detailed design of these systems, with regard to the tritium inventory, to eliminate all possible biological hazards caused by unforseen vent paths.

The questions of mechanical stability and vibration sensitivity have been considered in the design of the support structures. Mechanical movements during pulses and the steady expansion over a working day can be absorbed by bellows arrangements and sliding joints, but the large displacements and thermal conduction during bakeout will present problems. It may be necessary to mechanically decouple the spectrometer array from the torus during such periods. A platform with personnel access from the torus hall floor will require to be constructed along the side face of the spectrometer array for adjustment, servicing, and film changes in the early stages of operation. No heavy lifting gear will be required during these operations, though the placement of the lead and concrete shielding prior to D-T operation will. After initial commissioning, most adjustments apart from film changes will be carried out remotely. Access to the torus hall for servicing and the frequency of film changes will of course be dictated by the running schedule of the machine.

When eventually film is replaced by photoelectric recording all adjustments will be accomplished remotely. In D-T operation the problems of remote servicing of active complex spectrometer parts seems intractable and the most convenient solution in the event of failure would be to completely replace the whole spectrometer with a standby, or one of the three redundant units from the non active phase. The shielding round the spectrometer would of course need to be partly dismantled for this task and a modular, interlocking structure is thus required for this.

10. CALIBRATION AND ANCILLARY REQUIREMENTS

Routine crystal calibration for sensitivity and diffraction width will be contracted out to Leicester University's double crystal spectrometer test facility. Integrated reflectivity measurements can be supplied for the single mean wavelength designated for the particular crystal, but calibration over a range of wavelengths tells more about the overall crystal quality and the reliability of the measurements. This test unit will also supply sensitivity calibrations of recording films and photoelectric detector units, and transmissions of foils over a range of wavelengths, where required. Combining these values will provide an accurate and flexible calibration of the diagnostic as a whole.

Final alignment and testing can be accomplished prior to installation on the torus with high-intensity hard x-ray sources such as standard x-ray crystallographic units. It is envisaged that a central calibration facility covering the whole spectral range from x-rays to visible might be set up. In-situ checks of the detector electronic systems can be accomplished efficiently with inexpensive high-speed electronic pulse systems. Checks on drift of sensitivity-calibration of crystals and detectors can be achieved conveniently with small, built-in radioactive test sources such as Fe^{55}.

Precise checks of the crystal bending and grinding accuracy over the full aperture width will need to be carried out prior to sensitivity calibrations. Contractual arrangements for the use of the interferometric surface-profile test rig at National Physical Laboratory are envisaged, preferably with the crystal supplier involved as well.

Ancillary requirements would also include comparators and automatic scanning microdensitometers for fast reduction of photographic plate data. Provision of darkroom facilities is also needed.

11. PROBLEM AREAS AND DEVELOPMENT WORK

Problem areas which can be identified include the following:-

(i) Resolution of the conflict between the strict vacuum specifications and experimental aperture sizes and spectrometer materials.

(ii) The detailed design of a tritium pumping system.

(iii) The inversion of intensity profiles from non-circular plasmas with the probability of a severely limited range of views.

(iv) Temperature rises during machine operation

Development work which could proceed during an initial period before detailed design work commenced could include the following:-

(i) Construction of the basic dispersion system and test on DITE or TFTR

(ii) An investigation of minimum volume shielding design for the active phase from detailed models of the neutron and gamma-ray fluxes.

(iii) An investigation of the effects of radiation damage on the detector system in high intensity neutron fluxes produced in experimental test facilities such as those at National Radiation Protection Board.

(iv) Construction and testing of a prototype detector system.

(v) Preliminary software for the analysis routines including the Abel and tomographic inversion. This could best be done in concert with other users requiring similar work and under the direction of the CODAS group.

TABLE 1

WAVELENGTHS OF X-RAY LINES RELEVANT TO JET DISCHARGES

ELEMENT	Z	TRANSITION	λ(Å)	$\Delta\lambda$ GROUP
Neon	10	X H-like 1s-2p	12.134	
		IX He-like $1s^2$-1s2p $^1P_1$	13.447	
		$^3P_1$	13.560	0.25
		VIII Li-like satellite $1s^2 2p$-1s$2p^2$	13.650	
Argon	18	XVIII H-like 1s-2p	3.735	
		XVII He-like $1s^2$-1s2p $^1P_1$	3.948	
		$^3P_1$	3.968	0.047
		XVI Li-like satellite	3.995	
Titanium	22	XXII H-like 1s-2p	2.50	
		XXI He-like $1s^2$-1s2p $^1P_1$	2.610	
		$^3P_1$	2.623	0.026
		3p $^1P_1$	2.20	
		XX Li-like satellite	2.636	
		Kα	2.75	
Chromium	24	XXIV H-like 1s-2p	2.10	
		XXIII He-like $1s^2$-1s2p $^1P_1$	2.182	
		$^3P_1$	2.192	0.020
		3p $^1P_1$	1.87	
		XXII Li-like satellite	2.202	
		Kα	2.29	
		XV Neon-like 2p-3d	18.497	
		"	18.782	
		"	19.015	
		" " 2p-3s	20.863	
		"	21.151	
		"	21.216	

continued overleaf

TABLE 1 cont.

ELEMENT	Z	TRANSITION	λ(Å)	Δλ GROUP
Iron	26	XXVI H-like 1s-2p	1.79	
		XXV He-like $1s^2$-1s2p $^1P_1$	1.850	0.016
		$^3P_1$	1.859	
		3p $^1P_1$	1.59	
		XXIV Li-like satellite	1.866	
		Kα	1.94	
		XVII Neon-like 2p-3d	15.013	
		"	15.260	
		"	15.453	
		" " 2p-3s	16.775	
		"	17.051	
		"	17.091	
Nickel	28	XXVIII H-like 1s-2p	1.54	
		XXVII He-like $1s^2$-1s2p $^1P_1$	1.588	0.013
		$^3P_1$	1.596	
		3p $^1P_1$	1.36	
		XXVI Li-like satellite	1.601	
		Kα	1.66	
		XIX Neon-like 2p-3d	12.420	
		"	12.641	
		"	12.805	
		" " 2p-3s	13.768	
		"	14.030	
Molybdenum	42	Kα	0.709	
		Lα	5.406	
		XXXIII Neon-like 2s-3p (P)	5.204	
		" (N)	4.980	

TABLE 2

DOPPLER WIDTHS OF SELECTED X-RAY LINES AT ION TEMPERATURES RELEVANT TO JET

ELEMENT	M_i a.m.u.	λ(Å)	T_i = 1000 (eV)		T_i = 2000 (eV)		T_i = 5000 (eV)		T_i = 10,000 (eV)	
			$\frac{\lambda}{d\lambda}$	$d\lambda$(Å)	$\frac{\lambda}{d\lambda}$	$d\lambda$(Å)	$\frac{\lambda}{d\lambda}$	$d\lambda$(Å)	$\frac{\lambda}{d\lambda}$	$d\lambda$(Å)
Ne	20.183	12.134	1840	0.0066	1300	0.0093	825	0.0148	582	0.0208
A	39.944	3.948	2590	0.0015	1830	0.0022	1160	0.0034	819	0.0048
Ti	47.90	2.61	2840	0.0009	2000	0.0013	1270	0.0021	897	0.0029
Cr	52.01	2.18	2960	0.0007	2090	0.0010	1320	0.0017	935	0.0023
Fe	55.85	1.85	3060	0.0006	2170	0.0009	1370	0.0014	969	0.0019
Ni	58.69	1.59	3140	0.0005	2220	0.0007	1400	0.0011	993	0.0016
Ni	58.69	12.420	3140	0.0040	2220	0.0056	1400	0.0089	993	0.0125
Mo	95.95	0.709	4014	0.0002	2838	0.0003	1795	0.0004	1269	0.0006

TABLE 3

PROPOSED CRYSTAL BATTERY STOCK

λ(Å), Z		θ_B^o							
		High Resolution				High Reflectivity			
		Crystal	Refln.	2d(Å)	(F)	Crystal	Refln.	2d(Å)	(F)
0.709	MoKα	Quartz	$(90\bar{9}3)$ 50.79	0.915	7.0	—			
		Quartz	$(22\bar{4}3)$	2.030	14.3	Ge	(440)	2.000	124
1.54	Ni H-like		49.34				50.35		
1.59	Fe $1s^2$-1s3p		51.56				52.66		
1.59	Ni He-like		51.50				52.60		
1.66	Ni Kα		54.86				56.10		
		Quartz	$(13\bar{4}0)$	2.360	18.4	Topaz	(400)	2.325	48
1.79	Fe H-like		49.33				50.34		
1.85	Fe He-like		51.62				52.72		
1.87	Cr $1s^2$-1s3p		52.41				53.54		
1.94	Fe Kα		55.29				56.55		
		Quartz	$(20\bar{2}3)$	2.750	28.2	Topaz	(303)	2.712	138
2.10	Cr H-like		49.79				50.75		
2.18	Cr He-like		52.44				53.50		
2.29	Cr Kα		56.38				57.61		
		Quartz	$(02\bar{2}2)$	3.343	18.5				
2.50	Ti H-like		48.40						
2,61	Ti He-like		51.33				—		
2.75	Ti Kα		55.35						
		Quartz	$(11\bar{2}0)$	4.913	17.3	Gypsum	(200)	5.190	
3.948	A He-like $^1P_1$		53.47				49.53		
3.968	A He-like $^3P_1$		53.87				49.87		
4.015	A Li-like sat.		54.81				50.68		
		Quartz	$(01\bar{1}1)$	6.686	29.0	Ge	(111)	6.533	154
4.980	Mo Ne-like		48.15				49.67		
5.204	Mo Ne-like		51.11				52.80		
5.406	Mo Lα		53.96				55.84		
		Beryl	$(10\bar{1}0)$	15.955	67	Gypsum	(020)	15.168	
12.134	Ne H-like		49.51				53.12		
13.447	Ne He-like		57.44						
12.420	Ni Ne-like 2p-3d		51.12				54.97		
12.611	Ni Ne-like 2p-3d		52.22				56.25		
12.805	Ni Ne-like 2p-3d		53.38				57.59		

TABLE 4

TYPICAL CRYSTAL DIFFRACTION WIDTHS, $d\theta_1$ (arc sec)

(Published values are usually (1, − 1) double crystal values and are divided by 2 in this Table for equivalent single crystal values).

Crystal and Reflection	λ(Å) 0.709	1.54	1.85	2.29	3.95	5.0
Ge (220) Persson	3	7	8	11	-	-
Ge (440) Persson	1	3	-	-	-	-
Ge (111) Alexandropoulos et al	7	18	20	25	35	46
Quartz ($10\bar{1}1$) Brogren	2	4.5	5.5	7	15	23
Quartz ($22\bar{4}3$) Adell et al	0.4	0.6	-	-	-	-
Quartz ($20\bar{2}3$) Adell et al	0.5	1.0	1.5	2.0	-	-
Quartz ($11\bar{2}0$) Adell et al	1.2	1.7	2.0	2.6	8.0	-
Topaz (400)	Burek gives $\lambda/d\lambda$ = 77,000 which at 53° gives a $d\theta_1$ value of 2 arc sec at 1.85 Å					
Topaz (303)	Burek gives $\lambda/d\lambda$ = 10,000 which at 53° gives a $d\theta_1$ value of 14 arc sec at 2.29 Å.					
Quartz ($20\bar{2}2$) ($90\bar{9}3$) ($13\bar{4}0$) Beryl ($10\bar{1}0$) Gypsum (200) (020)	NOT KNOWN					

ANNEXE

BROAD-BAND CRYSTAL SPECTROSCOPY, A SURVEY INSTRUMENT FOR THE NON-ACTIVE PHASE OF JET

An extremely simple crystal spectrometer based on the "De Broglie" convexly curved configuration, Fig.A1, could be used on JET. This configuration has proved useful as a survey instrument for other laboratory plasmas and is capable of photographic measurements, Fig.A2, and photoelectric recording using a microchannelplate and delay-line as a detector/readout system, Figs. A3 and A4 The physical size of the instrument is small, the whole spectrometer fitting in a cylindrical vacuum vessel of 500 mm diameter and 350 mm height. The complete apparatus could be implemented inexpensively (£90,000 see Appendix 2), the major proportion of the cost lying in the vacuum pumping requirements.

The De Broglie configuration using a curved mica or K A P crystal results in a true broad-band spectrometer covering the wavelength range 1 - 26Å in a single exposure, but the bandwidth is obtained at the expense of sensitivity. It is calculated (Appendix 1) that on a 10 second exposure (i.e. 1 full pulse length of JET) a photographic record of density 0.5 would be registered in the main impurity lines. Photoelectric recording is possible with time-resolution to 1 s with moderate counting statistics (∿ 3%). The low signal levels mean that neutron-and-gamma induced noise would preclude operation in the active phase even with substantial shielding. Wavelength resolving powers ∿ 1 part in 1000 are achieved typically.

A simple scanning system on a flexible bellows arrangement would enable one spectrometer to view all the minor radius of the plasma to a resolution of ∿ 20 cm through a vertical port. No alignment or setting-up procedures are required. The aperture into the torus vacuum system for field of view requirements would be no more than 100 mm diameter and the actual vacuum aperture would be stopped down to an entrance slit of dimensions 5 x 0.05 cm, which could also be covered with a thin isolating foil if desired.

This spectrometer's use is seen therefore as a long term monitor of x-ray spectral information with only moderate time-and wavelength-resolution. It is envisaged that only the initial hydrogen phase of operation could be monitored. Approximate line profile evaluation for Doppler-broadening measurements might be a bonus in regimes with T_i in the several kilovolt region.

Appendix I

Sensitivity

The photographic sensitivity relation for the "De Broglie" spectrometer viewing an extended source through a narrow slit is given by

$$\int D.dx = \frac{\tau.T(\lambda).P(\lambda).r\sin\theta.R_c.s.b.\ell}{4\pi\ L(L + t)} \int E(\lambda)d\lambda$$

where $\int E(\lambda)d\lambda$ erg/cm^3/s is the radiant power density of the plasma in a line of wavelength λ Å.

$\int D.dx$ is the integrated photographic density in the line, which equals $D_p.(dx)_{\frac{1}{2}}$ where D_p is the peak density and $(dx)_{\frac{1}{2}}$ is the measured FWHM of the line.

τ s is the exposure time.

$T(\lambda)$ is the % transmission of wavelength λ through the optical path and foils.

$P(\lambda)$ density.erg^{-1}.cm^2 is the photographic plate response factor for the emulsion concerned at wavelength λ.

r cm is the radius of curvature of the crystal

θ^o is the Bragg angle for wavelength λ in the crystal concerned.

R_c radian is the crystal integrated reflectivity at wavelength λ.

s cm is the slit width

b cm is the slit length

ℓ cm is the depth of the viewed plasma volume.

L cm is the distance from slit to crystal.

t cm is the distance from crystal to film.

Consider the case of the Ni XXVII He-like $1s^2$-$1s2p\ ^1P_1$ line at 1.59 Å. A thin quartz $(22\bar{4}3)$ or germanium (220) crystal curved to a radius of 5.0 cm will view the plasma through a slit of dimensions 5.0 x 0.05 cm situated 50 cm from the crystal pole. Such a crystal would have an integrated reflectivity $\sim 10^{-4}$ radian for high-reflectivity recording, registering the line at a Bragg angle of 50^o. X-ray film has a plate response factor of 1.6 density.erg^{-1}.cm^2 for this wavelength and the exposure time is taken as the full 10 s pulse

length. An estimate of the radiant power density in this line can be obtained for JET conditions from calculations of Mertz, Cowan and Magee. Their results for the equivalent Fe XXV line for a 0.01 x n_e doping of iron in a plasma with $n_e = 10^{14}$ cm^{-3} and T_e = 2.0 keV give a power loss of 2.3 x 10^5 erg/cm^3/s. Scaling to JET parameters of $n_e = 3 \times 10^{13}$ cm^{-3} and a 0.001 x n_e doping for the same temperature gives a figure of 2.1 x 10^3 erg/cm^3/s. The measured line width $(dx)_{\frac{1}{2}}$ will approximate the slit function f(s) = Rs/L for the particular demagnification involved in the recording optics. Where the radius of the recording film plane is R = 15 cm, f(s) = 15 x 0.05/50 = 0.02 cm. The depth of the emitting volume is taken as 125 cm corresponding to a hot core of radius a/2. The distance t is approximately 10 cm in this example.

The maximum photographic density expected is then -

$$D_p = \frac{10.0 \times 1.0 \times 1.6 \times 5.0 \sin 50^o \times 10^{-4} \times 5.0 \times 0.05 \times 125 \times 2 \times 10^3}{4\pi \times 50 \times 60 \times 0.02}$$

$$= 0.51$$

Photoelectrically the energy density in the line (of width $(dx)_{\frac{1}{2}}$ normal to the detector face) is

$$W = \frac{\tau.T(\lambda).r\sin\theta.R_c.s.b.\ell}{4\pi\ L(L + t).(dx)_{\frac{1}{2}}} \int E(\lambda)d\lambda \quad \text{erg/cm}^2$$

For photons of energy hν erg the photon density is then

$$U = \frac{\tau.T(\lambda).r\sin\theta.R_c.s.b.\ell}{4\pi\ L(L+t).h\nu.(dx)_{\frac{1}{2}}} \int E(\lambda)d\lambda \quad \text{quanta/cm}^2$$

and the flux density

$$P = \frac{T(\lambda).r\sin\theta.R_c.s.b.\ell}{4\pi\ L(L+t).h\nu.(dx)_{\frac{1}{2}}} \int E(\lambda)d\lambda \quad \text{quanta/cm}^2\text{/s}$$

For a detector of height ℓ' the flux in the line is

$$F = \frac{T(\lambda).r\sin\theta.R_c.s.b.\ell.\ell'}{4\pi\ L(L+t).h\nu} \int E(\lambda)d\lambda \quad \text{quanta/s}$$

For the above conditions and a detector of height 1.0 cm, the flux expected in the line (hν = 1.24 x 10^{-8} erg) is

$$F = \frac{1.0 \times 5.0 \sin 50^o \times 10^{-4} \times 5.0 \times 0.05 \times 125 \times 1.0 \times 2 \times 10^3}{4\pi \times 50 \times 60 \times 1.24 \times 10^{-8}}$$

$$= 5 \times 10^4 \text{ quanta/s} \qquad (2.5 \times 10^6 \text{ quanta/cm}^2\text{/s})$$

At a detection efficiency of 2% this represents a counting rate in the readout system of 10^3 Hz. The global counting rate limit of the system is $\sim 5 \times 10^5$ Hz, so many hundreds of lines of this intensity could be recorded without distortion.

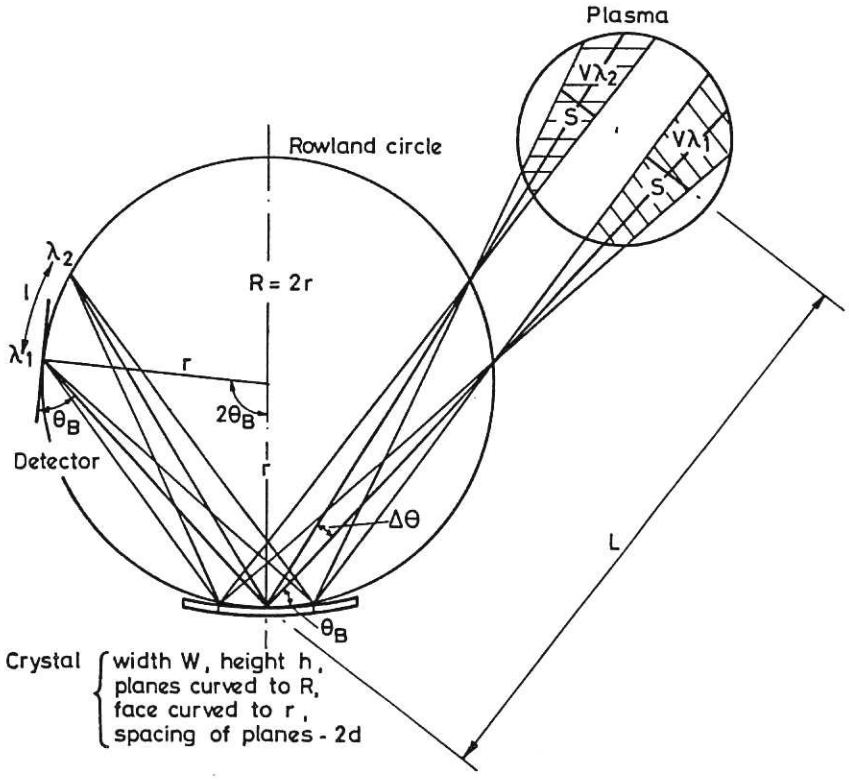

Fig.1 Schematic diagram of the optical principles of the Johansson mounting focussing crystal spectrometer.

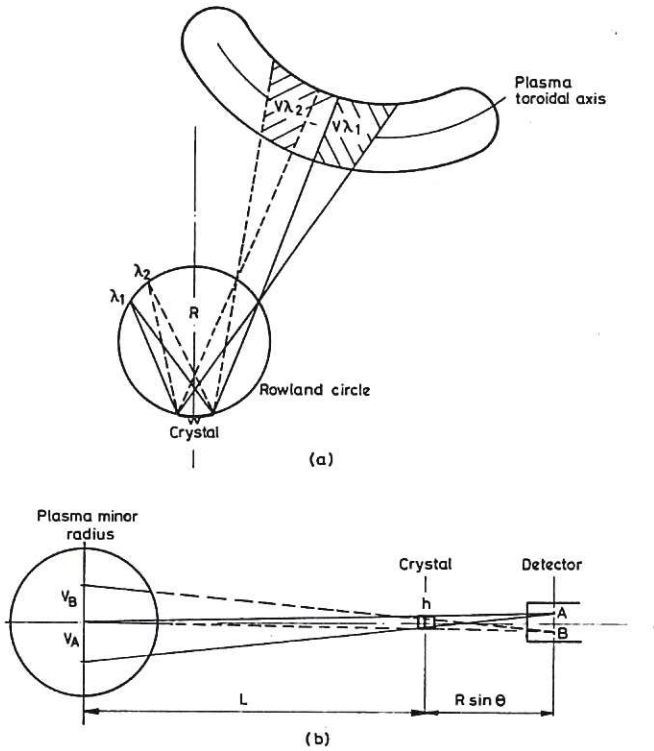

Fig.2 Observation with Rowland circle axis perpendicular to plasma toroidal axis. (a) Plan view showing alteration of field with wavelength. (b) Section showing space-resolution along a recorded line.

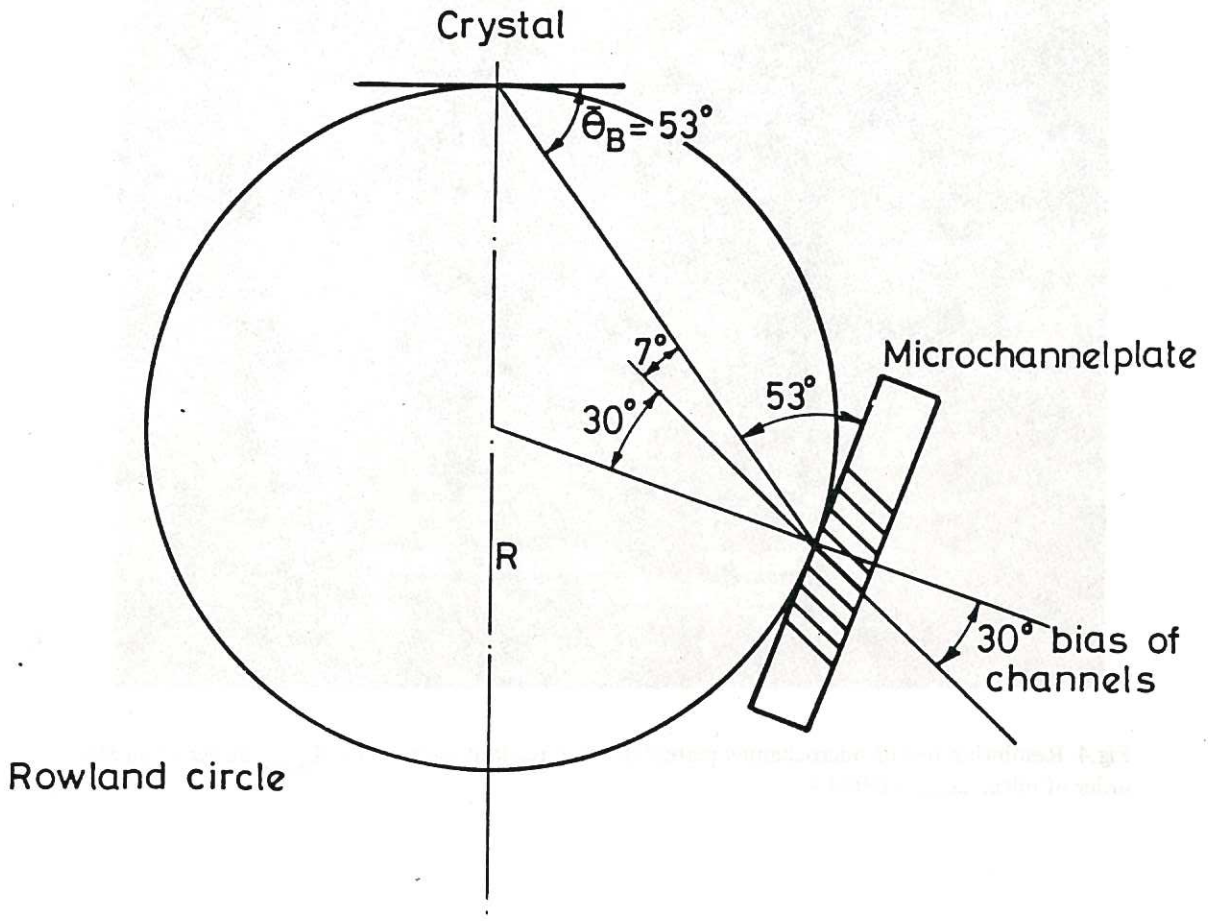

Fig.3 Tangential setting of special 30° bias microchannel plate for optimum efficiency (glancing angle 7°).

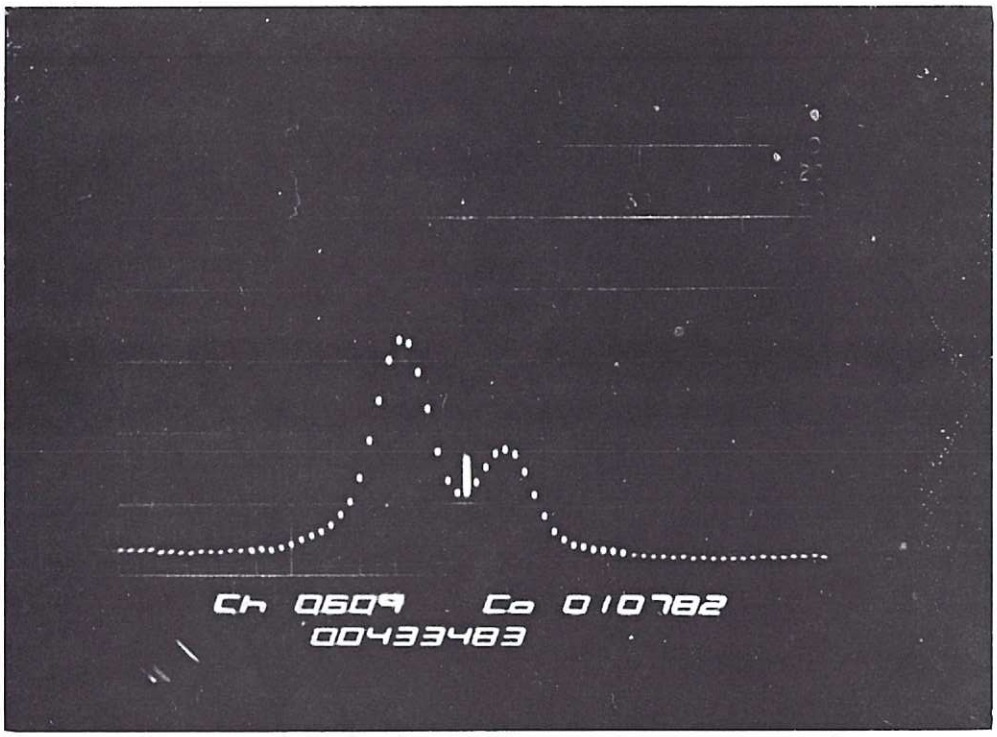

Fig.4 Resolution test of microchannel plate/delay line readout system. Cu $K_{\alpha_1 \alpha_2}$ dispersed in 5th order of mica. Δ_{sep} = 0·004 Å.

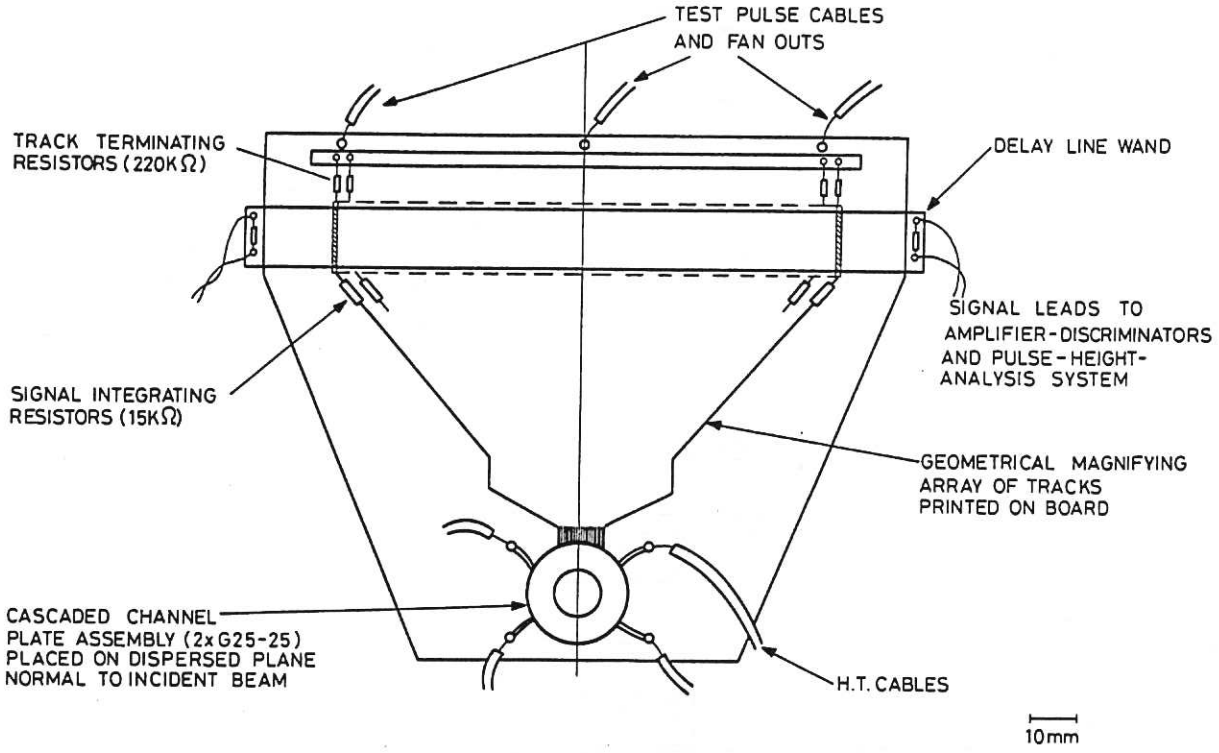

Fig.5 Schematic diagram of microchannel plate delay line readout assembly.

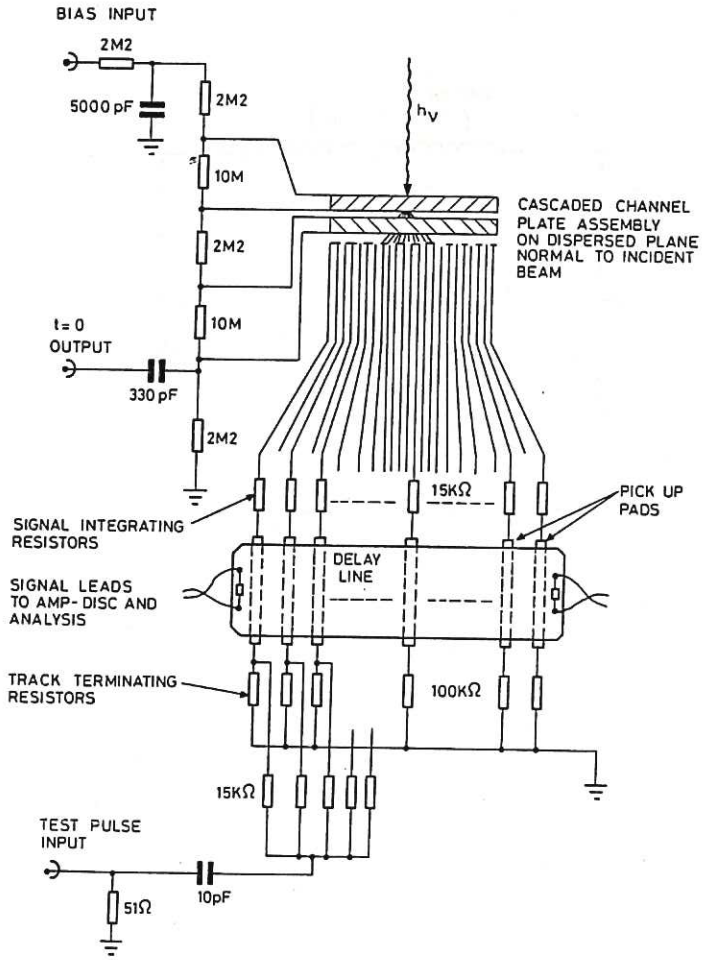

Fig.6 Microchannel plate readout electronics showing DC bias and test-pulse networks.

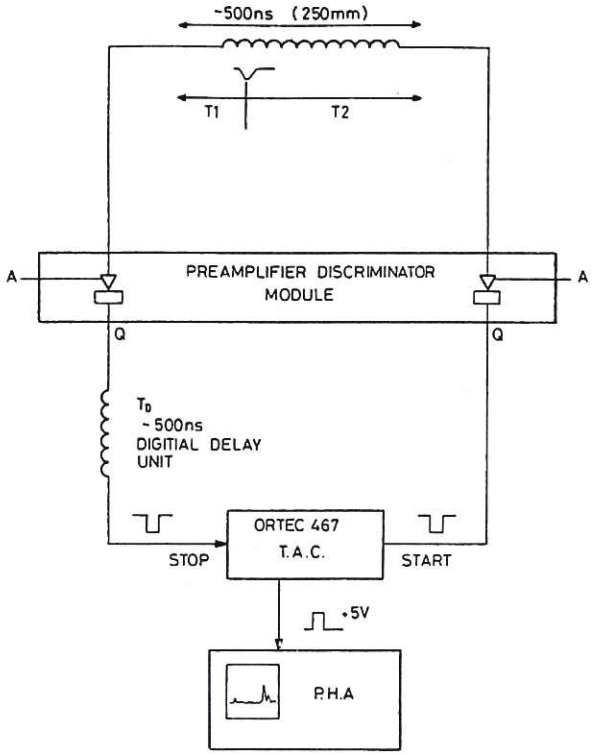

Fig.7 Schematic diagram of electronics used to record the X-ray spectrum.

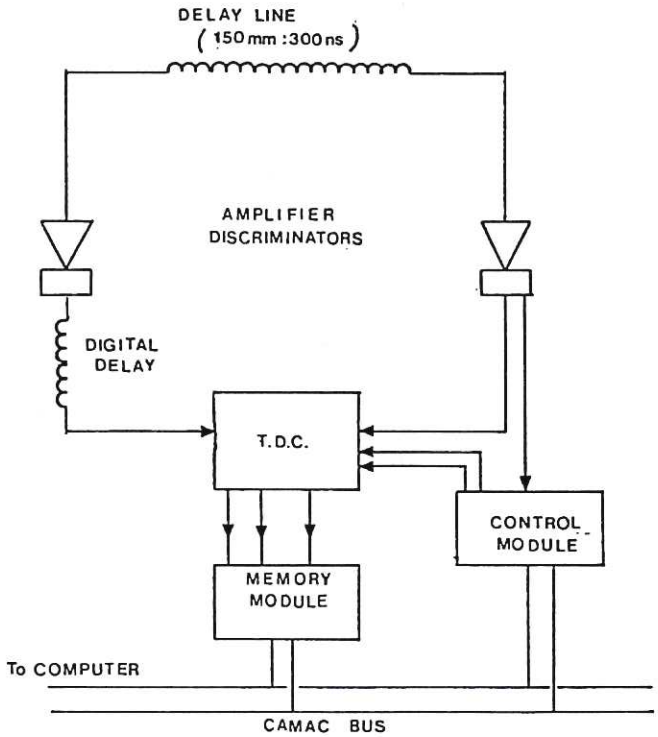

Fig.8 Schematic diagram of data capture and data storage electronics. The control module acting on the T.D.C. (Time Digital Converter) selects the time sample and spectral bandwidth so as to make optimum use of the memory module capacity.

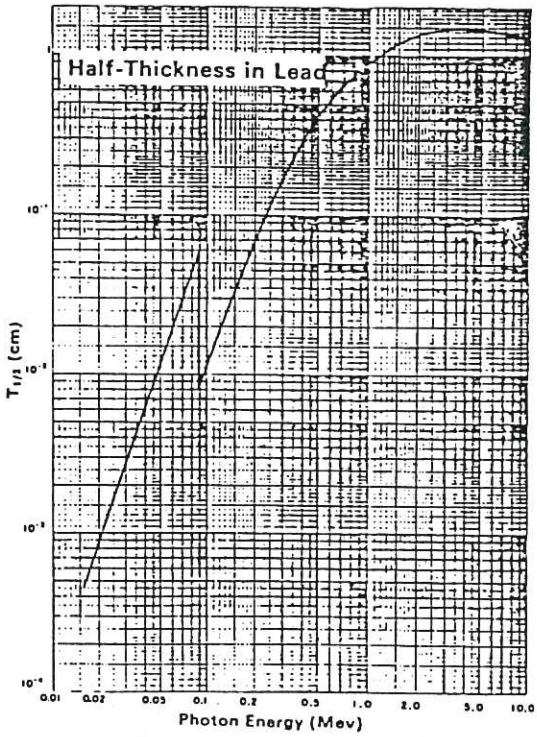

Fig.9 Half-thickness vs. photon energy for lead. (Centimeters of lead of density 11·29 g/cm^3 necessary to reduce the number of gamma rays in a broad beam by a factor of 2.)

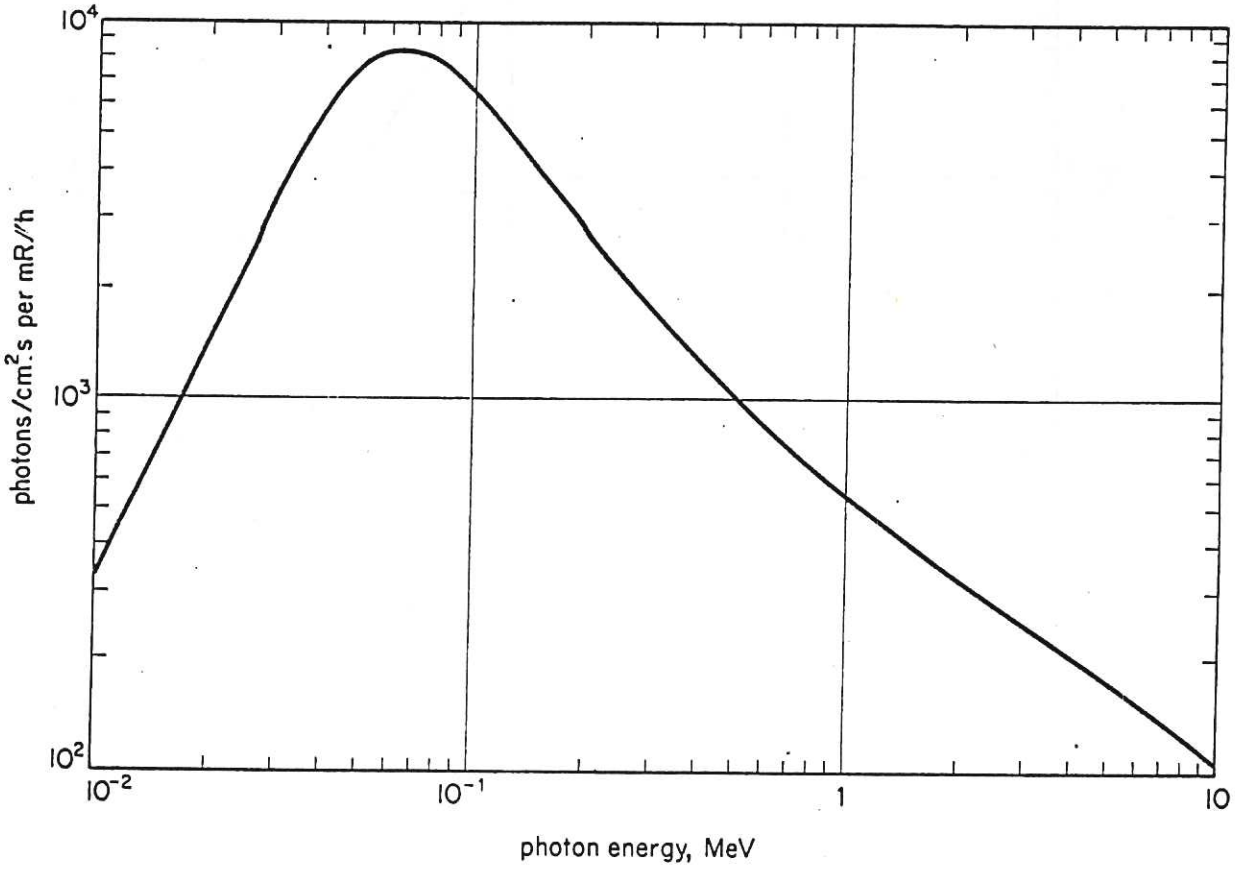

Fig.10 Relationship between photon fluence rate and exposure rate.

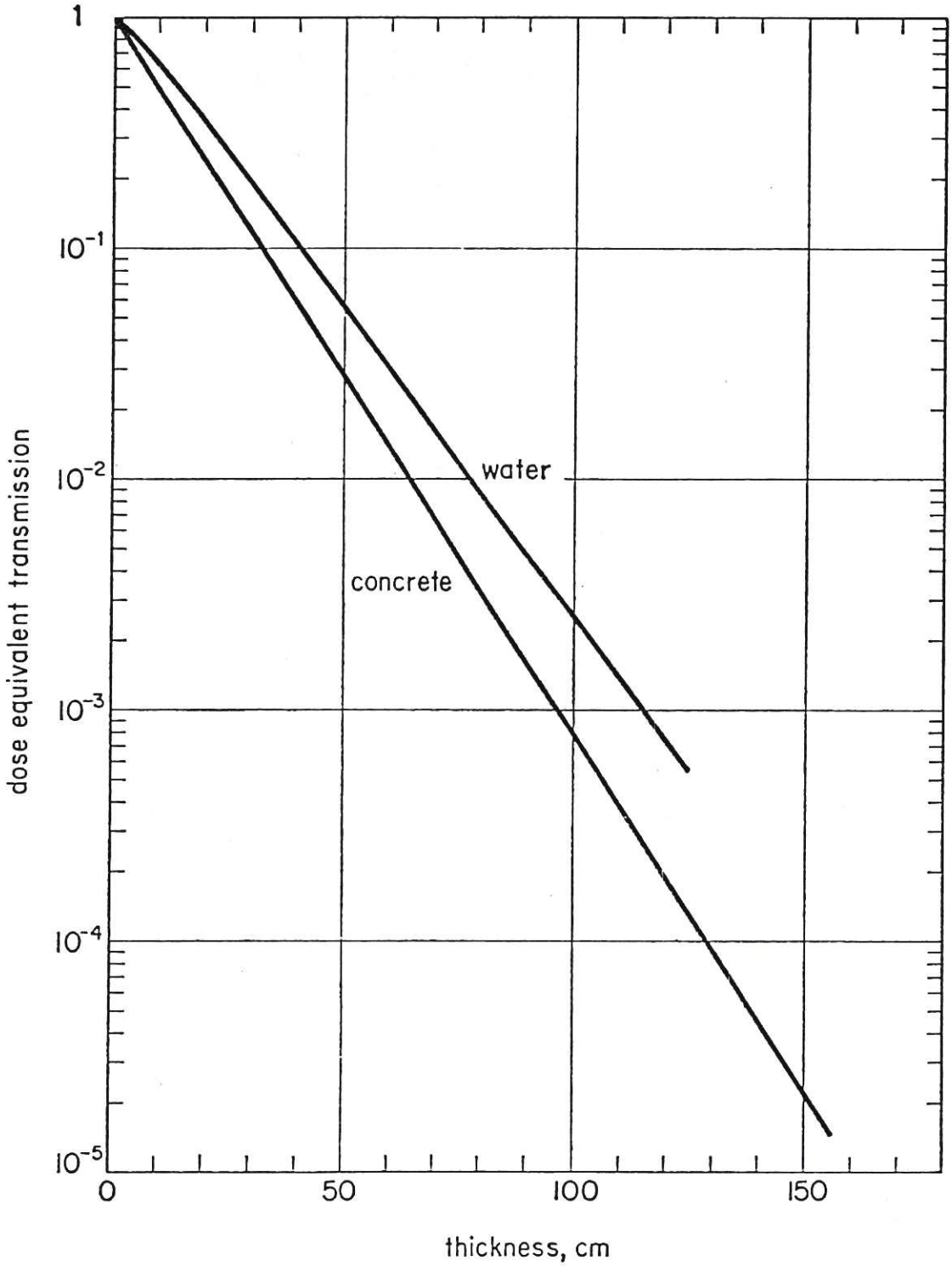

Fig.11 Broad-beam dose equivalent transmission of 14–15 MeV neutrons through slabs of concrete, density 2·4 g/cm^3, and water.

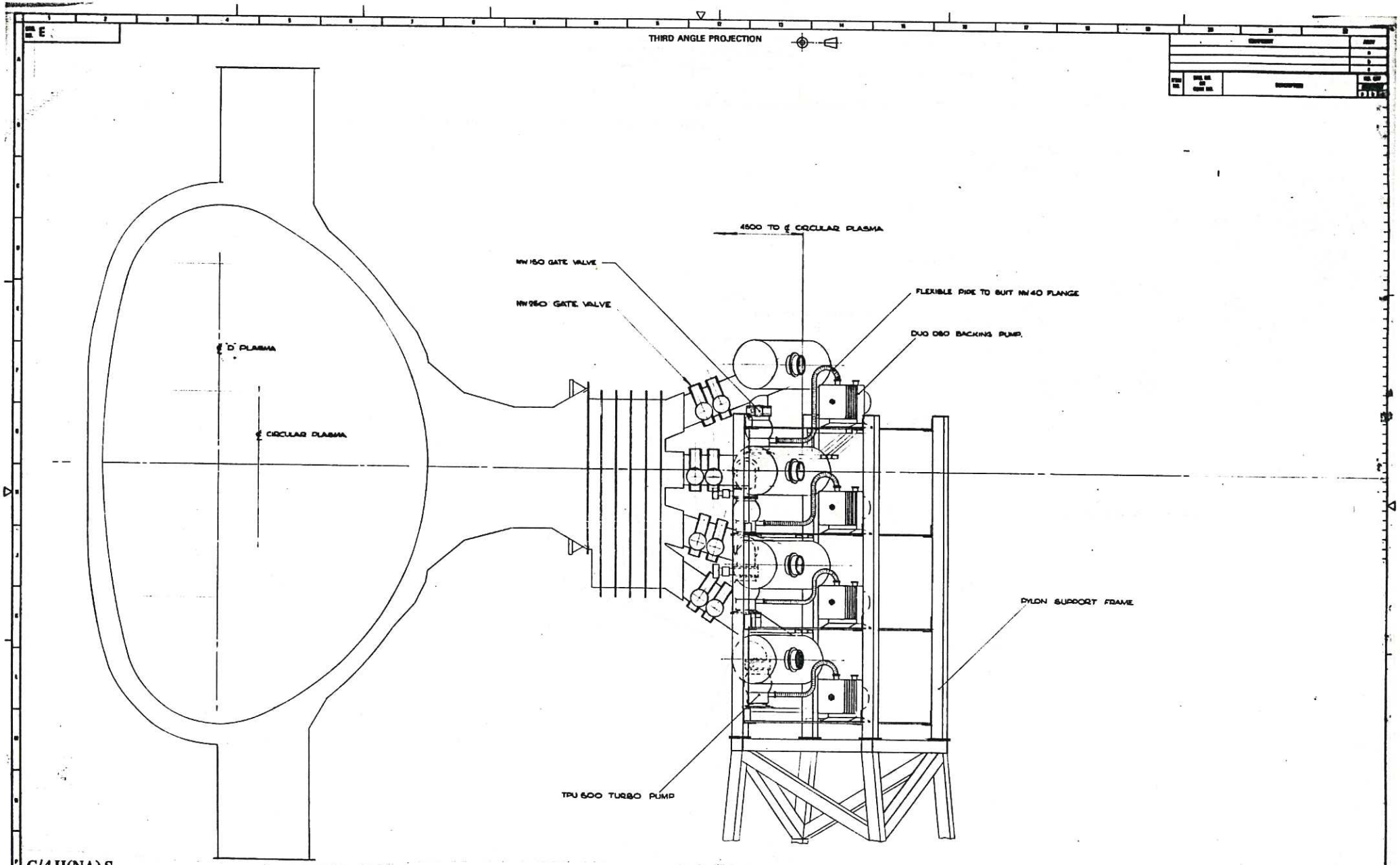

C/4 H(NA) S

Proposed layout (side view) of an array of four crystal spectrometers viewing the JET plasma in a horizontal direction (non-active operational phase).

CLM-R 203

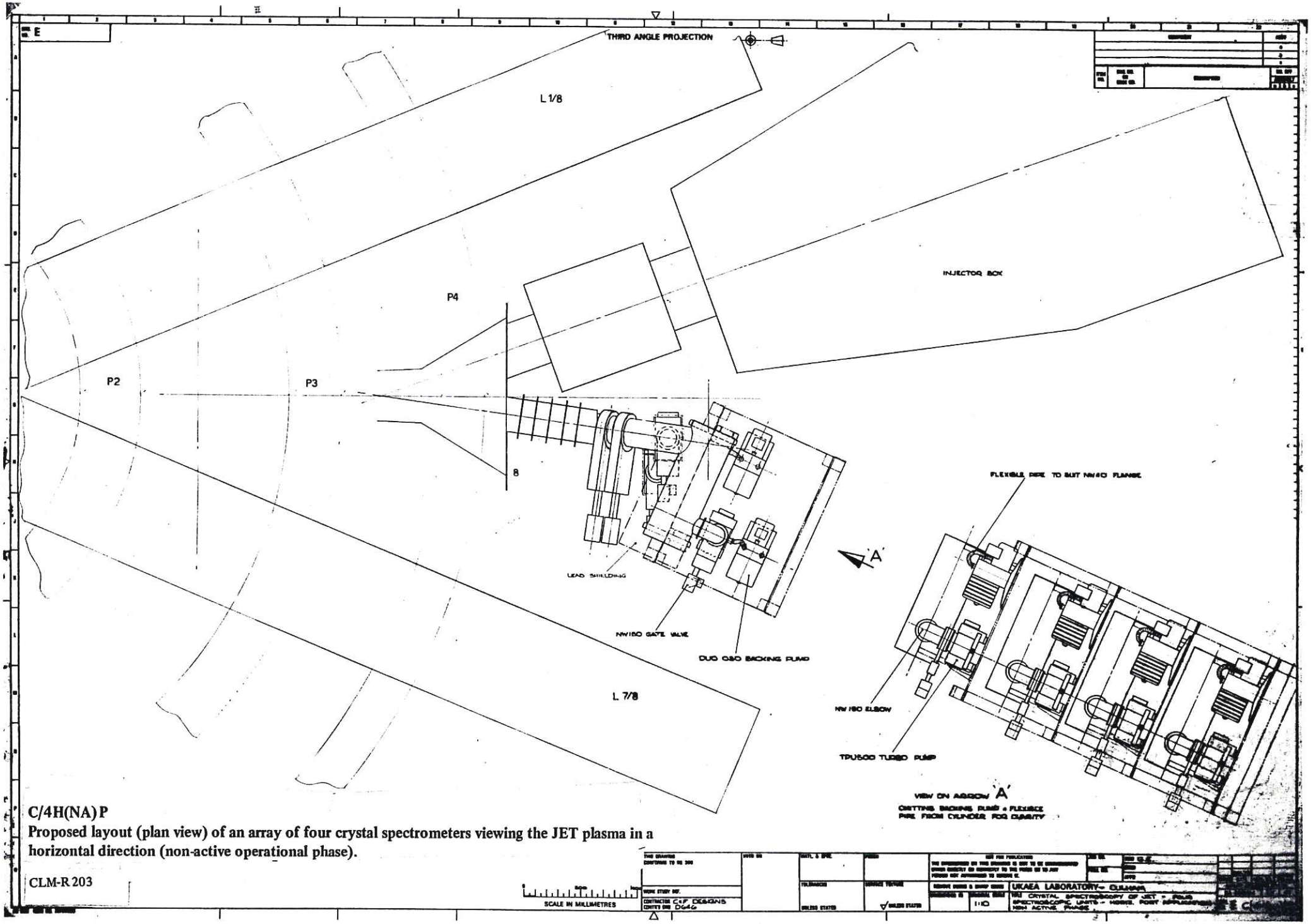

C/4H(NA) P

Proposed layout (plan view) of an array of four crystal spectrometers viewing the JET plasma in a horizontal direction (non-active operational phase).

CLM-R 203

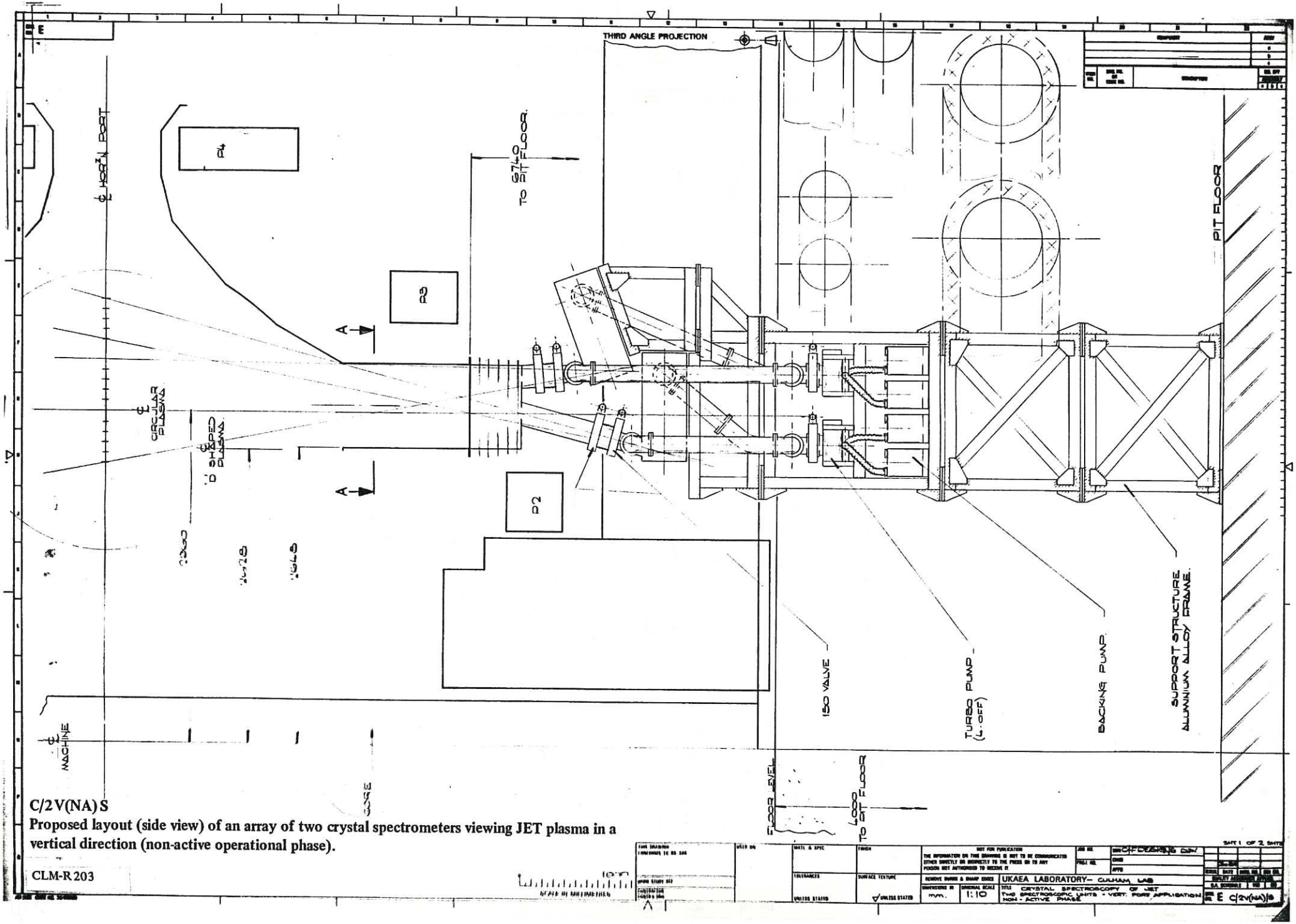

C/2V(NA) S

Proposed layout (side view) of an array of two crystal spectrometers viewing JET plasma in a vertical direction (non-active operational phase).

CLM-R 203

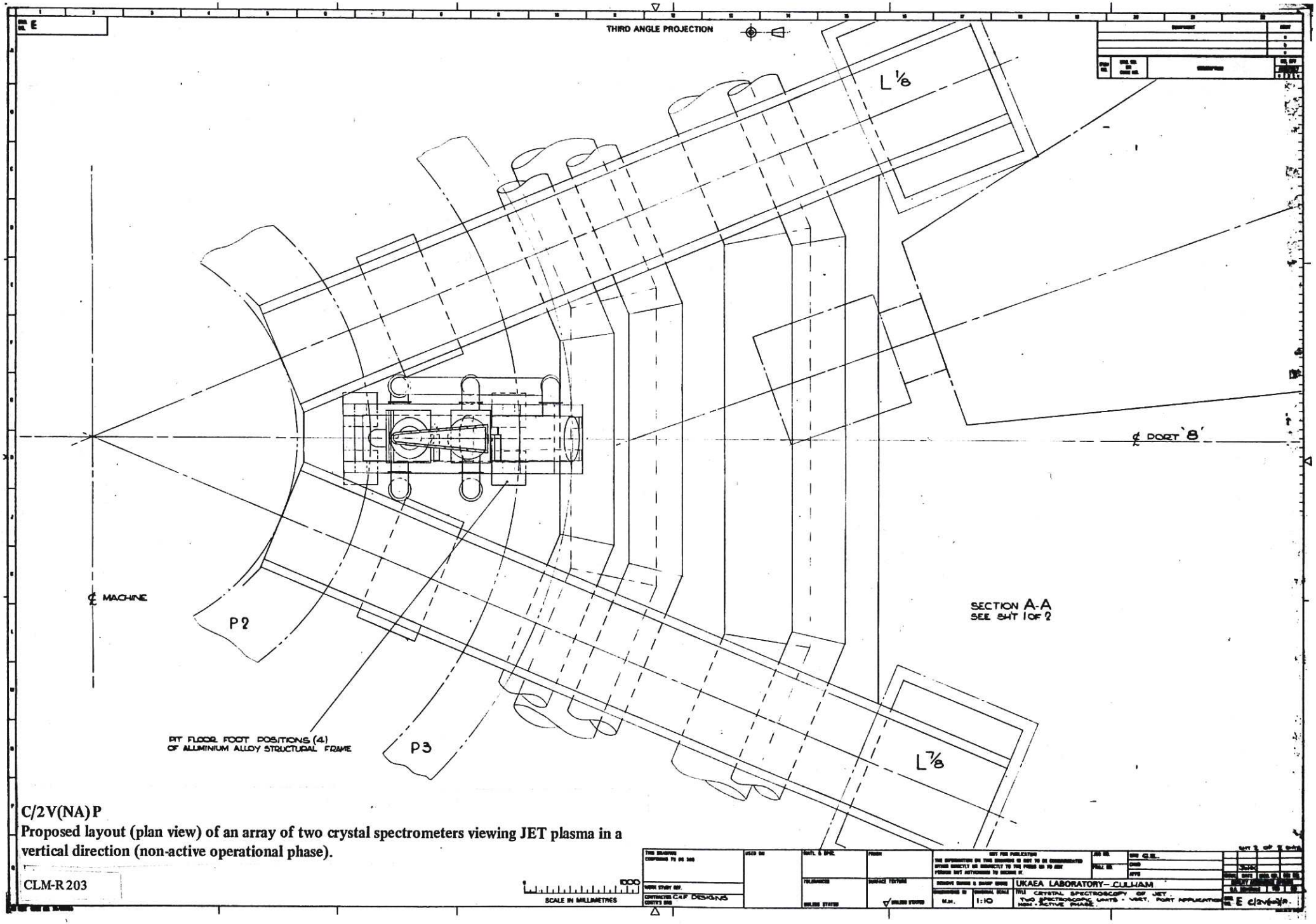

C/2V(NA)P

Proposed layout (plan view) of an array of two crystal spectrometers viewing JET plasma in a vertical direction (non-active operational phase).

CLM-R 203

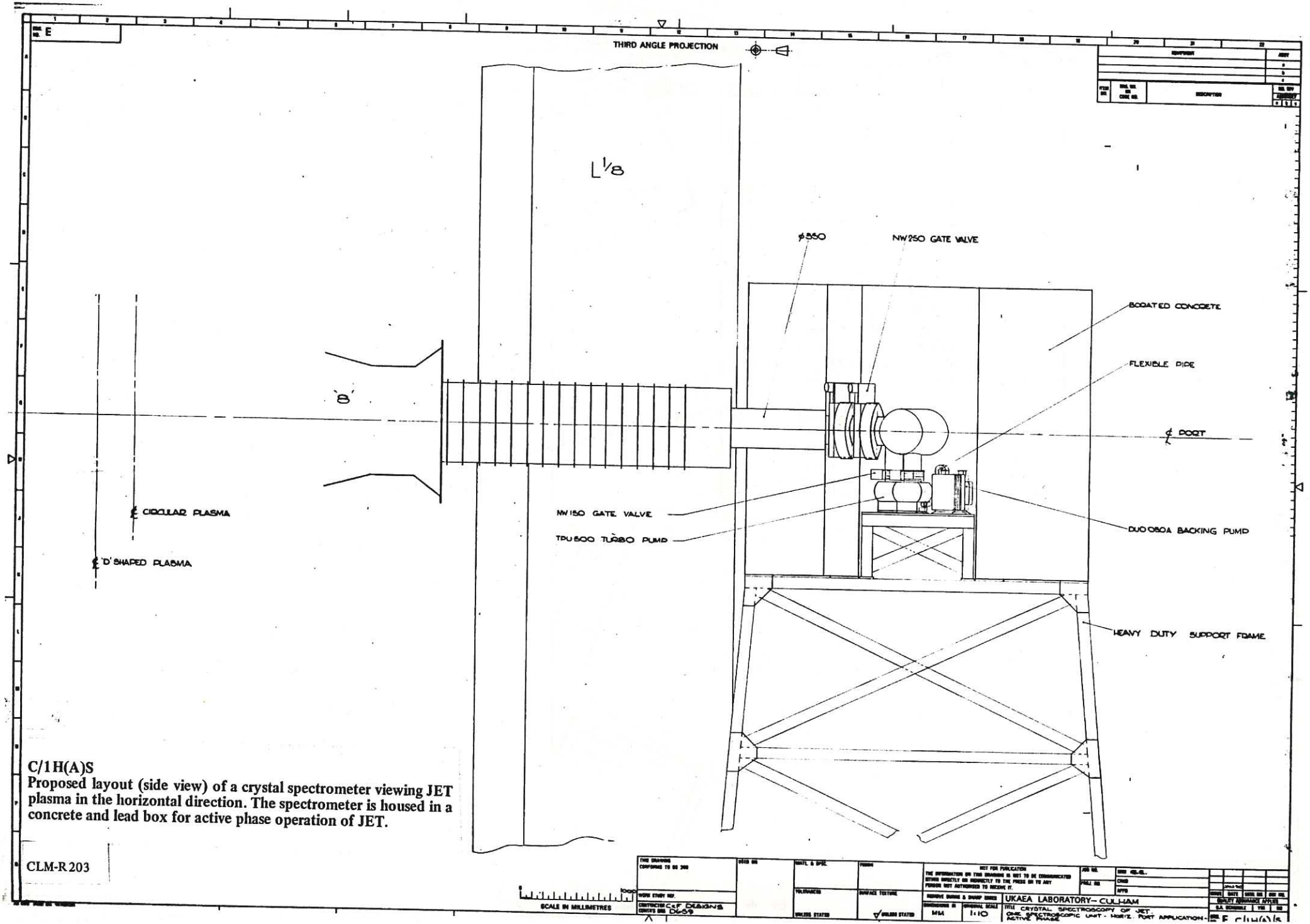

C/1H(A)S
Proposed layout (side view) of a crystal spectrometer viewing JET plasma in the horizontal direction. The spectrometer is housed in a concrete and lead box for active phase operation of JET.

CLM-R 203

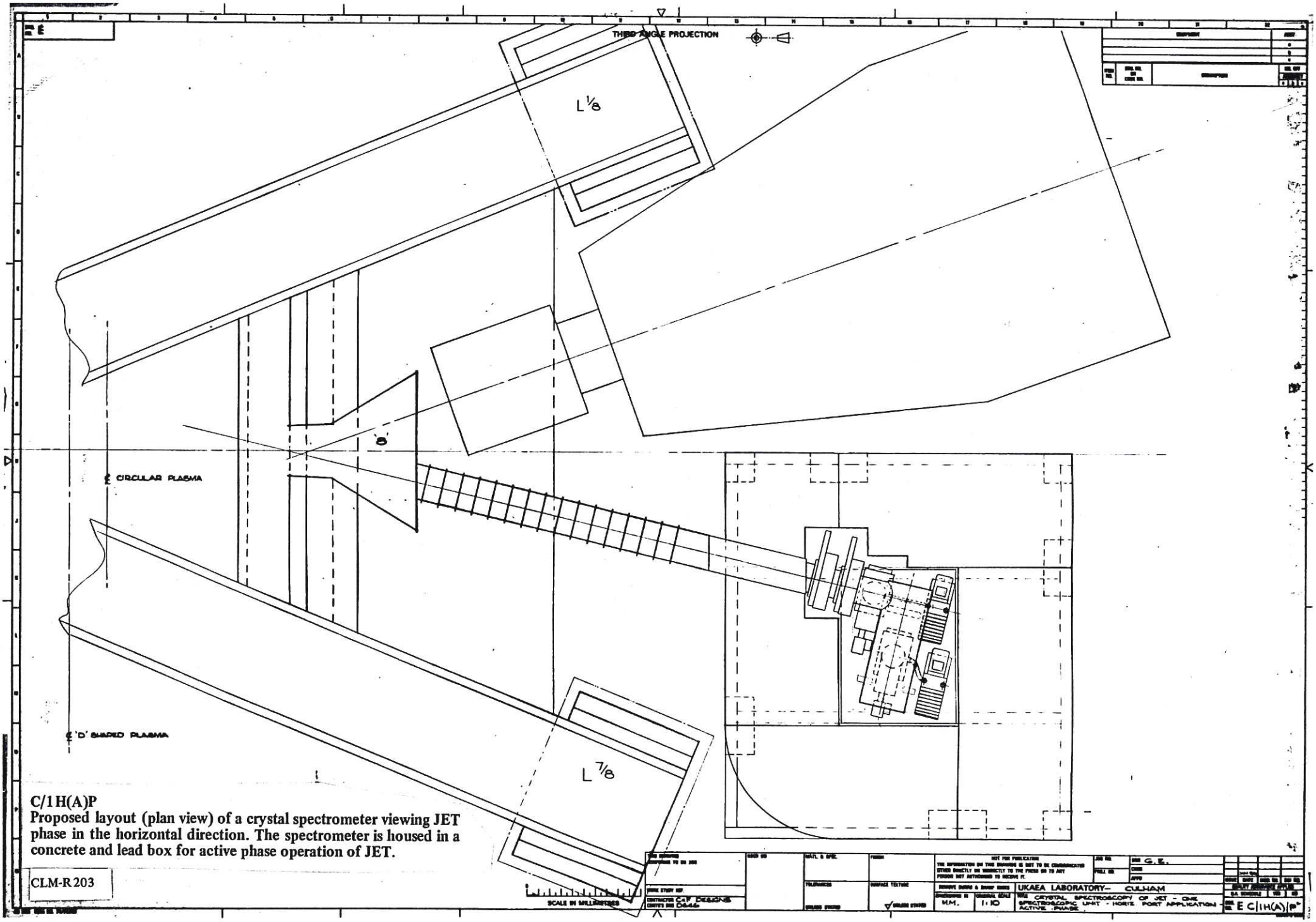

C/1H(A)P
Proposed layout (plan view) of a crystal spectrometer viewing JET phase in the horizontal direction. The spectrometer is housed in a concrete and lead box for active phase operation of JET.

CLM-R203

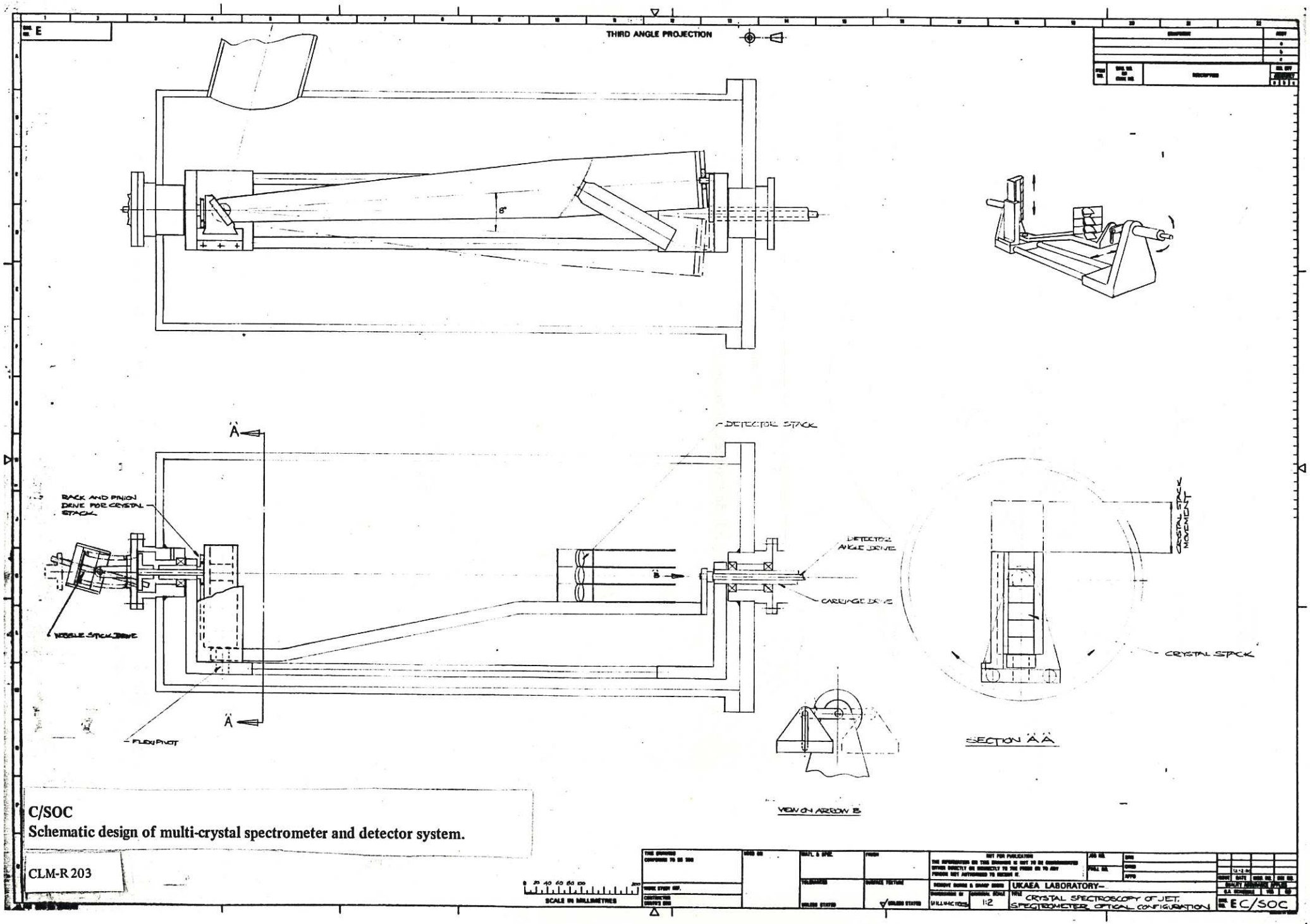

C/SOC

Schematic design of multi-crystal spectrometer and detector system.

CLM-R 203

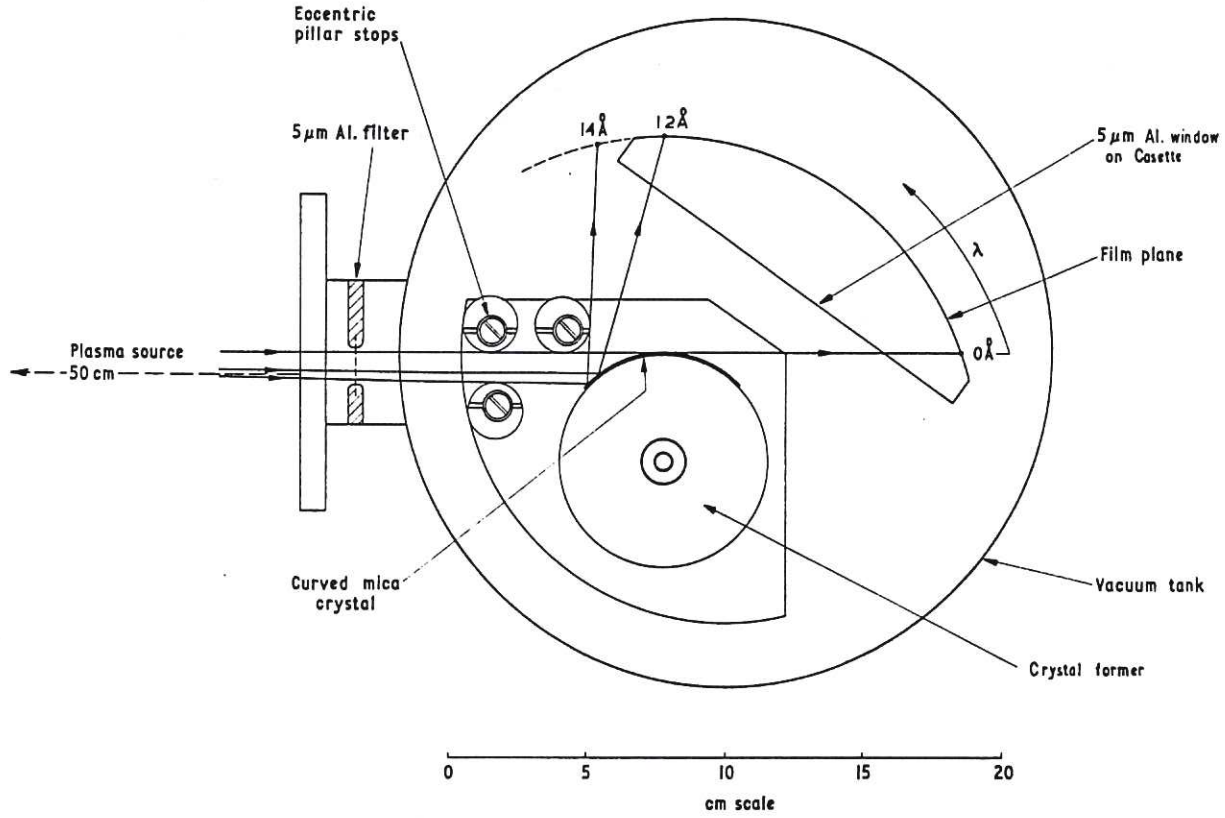

Fig.A1 de Broglie spectrometer.

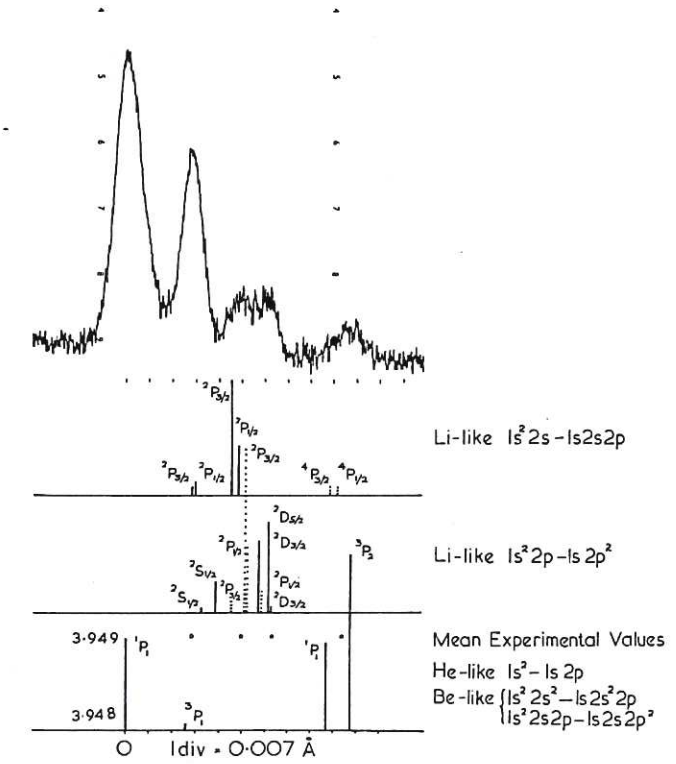

Fig.A2 Calculated Li-like multiplet structure of argon compared with plasma focus spectrum (4% A in 2·5 torr D_2 ; 23 kV).

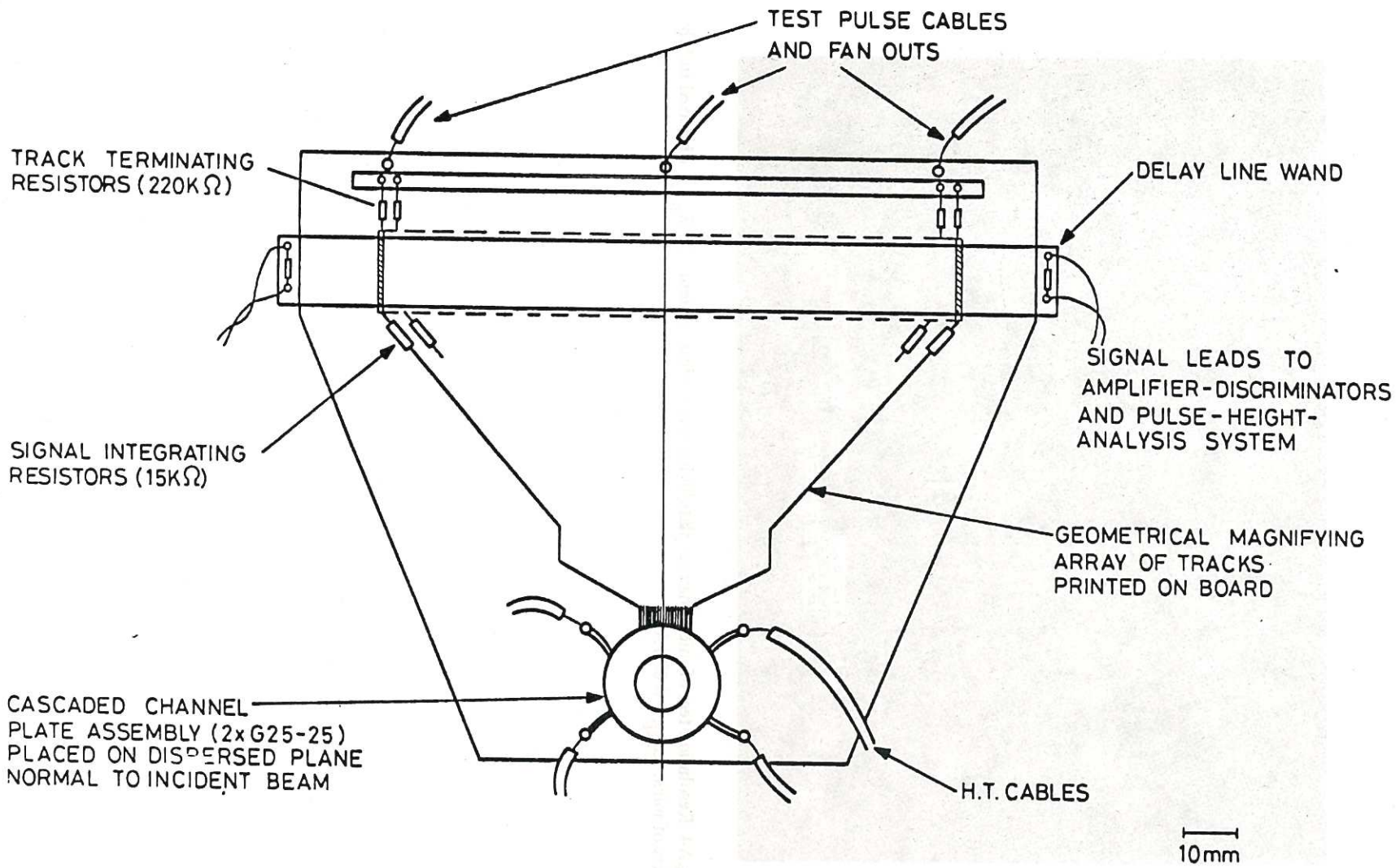

Fig.A3 Schematic diagram of microchannel plate delay line readout assembly.

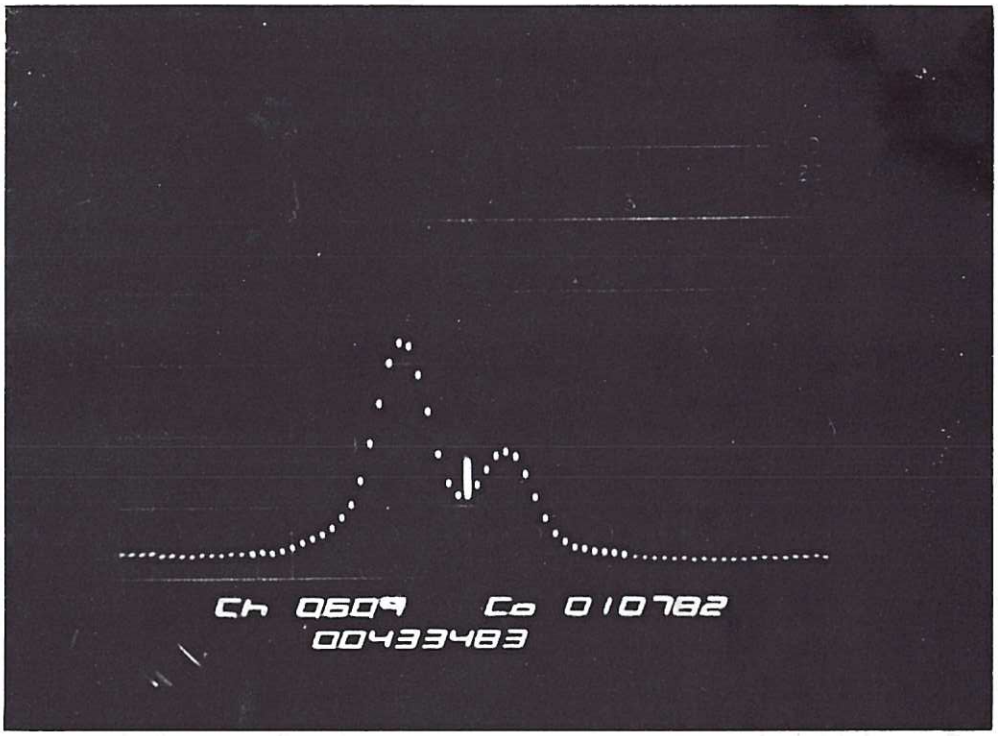

Fig.A4 Resolution test of microchannel plate/delay line readout system. Cu $K_{\alpha_1\alpha_2}$ dispersed in 5th order of mica. Δ_{sep} = 0·004 Å.

HER MAJESTY'S STATIONERY OFFICE

Government Bookshops

49 High Holborn, London WC1V 6HB
13a Castle Street, Edinburgh EH2 3AR
41 The Hayes, Cardiff CF1 1JW
Brazennose Street, Manchester M60 8AS
Wine Street, Bristol BS1 2BQ
258 Broad Street, Birmingham B1 2HE
80 Chichester Street, Belfast BT1 4JY

Government publications are also available through booksellers